cmgh
CELLULAR AND MOLECULAR GASTROENTEROLOGY AND HEPATOLOGY

ORIGINAL RESEARCH

Programmed Death Ligand 1-Expressing Classical Dendritic Cells Mitigate *Helicobacter*-Induced Gastritis

Du-Min Go,[1,*] Seung Hyun Lee,[2,*] Su-Hyung Lee,[3] Sang-Ho Woo,[1] Kibyeong Kim,[2] Kyeongdae Kim,[2] Kyu Seong Park,[2] Jong-Hwan Park,[4] Sang-Jun Ha,[5] Woo Ho Kim,[6] Jae-Hoon Choi,[2] and Dae-Yong Kim[1]

[1]*Department of Veterinary Pathology, College of Veterinary Medicine, Seoul National University, Seoul, Republic of Korea;* [2]*Department of Life Sciences, College of Natural Sciences, Research Institute for Natural Sciences, Hanyang University, Seoul, Republic of Korea;* [3]*Division of Cancer Biology, Research Institute of National Cancer Center, Gyeonggi-do, Republic of Korea;* [4]*Laboratory Animal Medicine, College of Veterinary Medicine, Chonnam National University, Gwangju, Republic of Korea;* [5]*Department of Biochemistry, College of Life Science and Biotechnology, Yonsei University, Seoul, Republic of Korea;* [6]*Department of Pathology, College of Medicine, Seoul National University, Seoul, Republic of Korea*

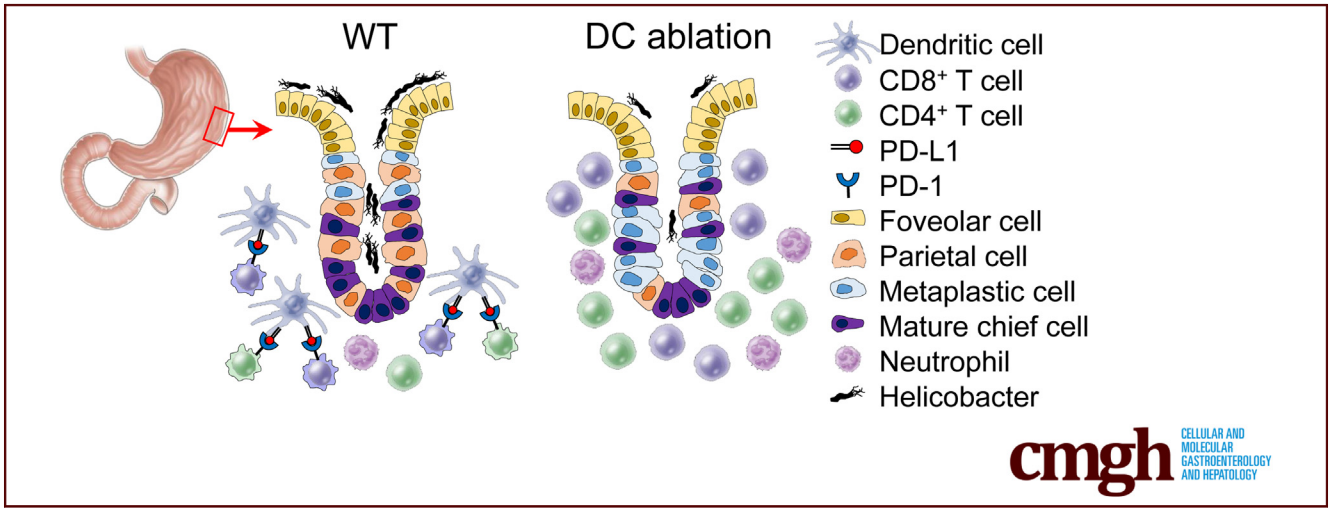

SUMMARY

The induced programmed cell death ligand 1 expression in gastric epithelium has been suggested as an immunomodulatory mechanism for persistent gastric *Helicobacter* colonization. In this study, we found that classical dendritic cells mainly express programmed cell death ligand 1 in the gastric mucosal area and play a pivotal role in *Helicobacter*-induced gastritis.

BACKGROUND & AIMS: *Helicobacter pylori* has been reported to modulate local immune responses to colonize persistently in gastric mucosa. Although the induced expression of programmed cell death ligand 1 (PD-L1) has been suggested as an immune modulatory mechanism for persistent infection of *H pylori*, the main immune cells expressing PD-L1 and their functions in *Helicobacter*-induced gastritis still remain to be elucidated.

METHODS: The blockades of PD-L1 with antibody or PD-L1–deficient bone marrow transplantation were performed in *Helicobacter*-infected mice. The main immune cells expressing PD-L1 in *Helicobacter*-infected stomach were determined by flow cytometry and immunofluorescence staining. *Helicobacter felis* or *H pylori*–infected dendritic cell (DC)-deficient mouse models including *Flt3*$^{-/-}$, *Zbtb46*–diphtheria toxin receptor, and *BDCA2*–diphtheria toxin receptor mice were analyzed for pathologic changes and colonization levels. Finally, the location of PD-L1–expressing DCs and the correlation with *H pylori* infection were analyzed in human gastric tissues using multiplexed immunohistochemistry.

RESULTS: Genetic or antibody-mediated blockade of PD-L1 aggravated *Helicobacter*-induced gastritis with mucosal metaplasia. Gastric classical DCs expressed considerably higher levels of PD-L1 than other immune cells and co-localized with T cells in gastritis lesions from *Helicobacter*-infected mice and human beings. *H felis*– or *H pylori*–infected *Flt3*$^{-/-}$ or classical DC-depleted mice showed aggravated gastritis with severe T-cell and neutrophil accumulation with low bacterial loads compared with that in control mice. Finally, PD-L1–expressing DCs were co-localized with T cells and showed a positive correlation with *H pylori* infection in human subjects.

CONCLUSIONS: The PD-1/PD-L1 pathway may be responsible for the immune modulatory function of gastric DCs that

protects the gastric mucosa from *Helicobacter*-induced inflammation, but allows persistent *Helicobacter* colonization. *(Cell Mol Gastroenterol Hepatol 2021;12:715–739; https://doi.org/10.1016/j.jcmgh.2021.04.007)*

Keywords: Gastric Inflammation; T Cell; Immune Regulation; Mucosal Metaplasia.

Programmed death-ligand 1 (PD-L1; CD274) is a co-inhibitory molecule of the B7 family ligands and indispensable for the maintenance of T-cell tolerance. PD-L1 suppresses T-cell activity by transferring inhibitory signals to T cells and interfering with T-cell stimulatory signals via programmed death 1 (PD-1; CD279) receptor.[1,2] Therefore, PD-1/PD-L1 signaling modulates T-cell–mediated immunity by regulating the number of T cells and their activity in multiple ways, for instance, by inducing T-cell exhaustion,[3] anergy,[4] apoptosis,[5] or inhibiting cell proliferation.[6] PD-1/PD-L1 interaction has been known to play a crucial role in tumor immune escape. Because PD-L1 on tumor cells suppresses antitumor T-cell response, PD-1/PD-L1 blockade has been considered a highly promising antitumor therapy. Meanwhile, PD-1/PD-L1 interaction also play important roles in various infectious diseases induced by virus, bacteria, or parasite.[7] The T cells that infiltrate into the site of inflammation with infectious agents are suppressed by PD-1/PD-L1 engagement, allowing persistent infection but preventing immune-mediated tissue damage.[8] Thus, the proper regulation of the PD-1/PD-L1 pathway appears to be very important to control inflammation and subsequent tissue damage during chronic infection.

Chronic infection of *Helicobacter pylori* causes persistent gastric inflammation. Approximately 50% of the human population is colonized by *H pylori*, 15% of whom develop severe lesions such as severe chronic gastritis, peptic ulcer, gastric adenocarcinoma, and lymphoma.[9] Interestingly, the majority of gastric cancers are associated with *H pylori*.[10] *H pylori*–induced gastropathy is affected mostly by the host's immune response against *H pylori*.[11] Various components of *H pylori* and signals from mucosal epithelial cells in contact with *H pylori* cause infiltration of innate immune cells including dendritic cells (DCs), macrophages, monocytes, and neutrophils. Although the responses of $CD4^+$ or $CD8^+$ T cells also are generated against *H pylori*,[9,12–14] these T-cell–mediated immune responses were not effective in eradicating colonized *H pylori* in the gastric mucosa.[15–17] T-cell–derived interferon-γ (IFN-γ) contributes to the development of severe gastritis and precancerous mucosal metaplasia.[18,19]

Previously, PD-1/PD-L1 has been reported to have a role in persistent gastric infection of *H pylori*. *H pylori* infection increases the PD-L1 expression on gastric epithelial cells and suppresses T-cell responses in gastric mucosa.[20,21] However, antigen-presenting cells such as DCs and macrophages can express a higher level of PD-L1,[8] and may play important roles in T-cell response to *H pylori*. Indeed, the PD-L1 expression of DCs was increased by *H pylori*, but its role still is unknown.[22] In this study, we attempted to analyze the effect of PD-L1 blockade on bacterial colonization, inflammation, and precancerous mucosal changes in *Helicobacter felis*–infected gastric mucosa. Interestingly, gastric DCs were the main PD-L1–expressing cells and co-localized with T cells in the gastric mucosa of *Helicobacter*-infected mice and human beings. The ablation of classical DCs (cDCs) also induced severe lymphocytic gastritis with suppression of *Helicobacter* colonization. Collectively, PD-L1–expressing cDCs attenuate mucosal inflammation and precancerous mucosal metaplasia, but support the persistent *Helicobacter* colonization by modulating T-cell response.

Results

Blockade of PD-L1 With Antibody or PD-L1 Deficiency in Bone Marrow–Derived Cells Enhance Gastric Inflammation With Mucosal Metaplasia Upon Helicobacter *Infection*

To confirm the role of PD-L1 in the host immune response to *Helicobacter* infection, we injected PD-L1 antibody (Ab) into *H felis*–infected wild-type (WT) mice to block PD-L1 signals. We analyzed gastric lesions at 4 weeks after infection. Histologically, lymphocyte infiltration into the gastric submucosa and mucosal lamina propria, as well as pathologic mucosal changes, were markedly more severe in the PD-L1 Ab–injected group than in the control Ab-injected group (Figure 1*A*). Furthermore, $CD3^+$ T-cell infiltration into the mucosal lamina propria was more prominent in the PD-L1 Ab–injected group (Figure 1*B*). We performed flow cytometry analysis to observe the changes of various leukocyte populations in the *H felis*–infected stomach (Figure 1*C*). Among the leukocyte populations, T-cell infiltration was increased markedly by PD-L1 Ab injection. Infiltration of $CD8^+$ T cells and $CD4^+$ T cells was more prominent in the PD-L1 Ab–injected group, whereas the percentage of regulatory T cells (Tregs) in $CD4^+$ T cells tended to be lower in the PD-L1 Ab–injected group (Figure 1*D*). The bacterial loads in the stomach were decreased in the PD-L1 Ab–injected group than in the control Ab-injected group (Figure 1*E*).

Several studies have reported PD-L1 expression on the gastric mucosal epithelium during *Helicobacter*

*Authors share co-first authorship

Abbreviations used in this paper: **Ab, antibody; ATPase, adenosine triphosphatase; BM, bone marrow; BMT, bone marrow transplanted; cDC, classical dendritic cell; CLU, clusterin; DC, dendritic cell; DN, double-negative; DT, diphtheria toxin; DTR, diphtheria toxin receptor; FBS, fetal bovine serum; Flt3, fms-like tyrosine kinase 3; IFN-γ, interferon-γ; IHC, immunohistochemistry; IL, interleukin; IRAE, immune-related adverse event; IRF, interferon regulatory factor; MHC, major histocompatibility complex; mRNA, messenger RNA; PCR, polymerase chain reaction; PD-1, programmed death 1; pDC, plasmacytoid DC; PD-L1, programmed death-ligand 1; SIRPα, signal regulatory protein alpha; SP-D, surfactant protein-D; SPEM, spasmolytic polypeptide-expressing metaplasia; TFF2, trefoil factor 2; Treg, regulatory T cell; WT, wild type; XCR1, X-C motif chemokine receptor 1; ZBTB46, zinc finger and BTB domain containing 46.**

Most current article

2352-345X
https://doi.org/10.1016/j.jcmgh.2021.04.007

infection.[20,21,23] However, various hematopoietic lineage cells also express PD-L1.[8] To determine the function of PD-L1 on hematopoietic lineage cells in *Helicobacter* infection, we created bone marrow (BM) chimeras by transplanting Cd274$^{-/-}$ (*Pdl1*$^{-/-}$) or WT BM into irradiated WT mice. Histologically, inflammatory lesions were

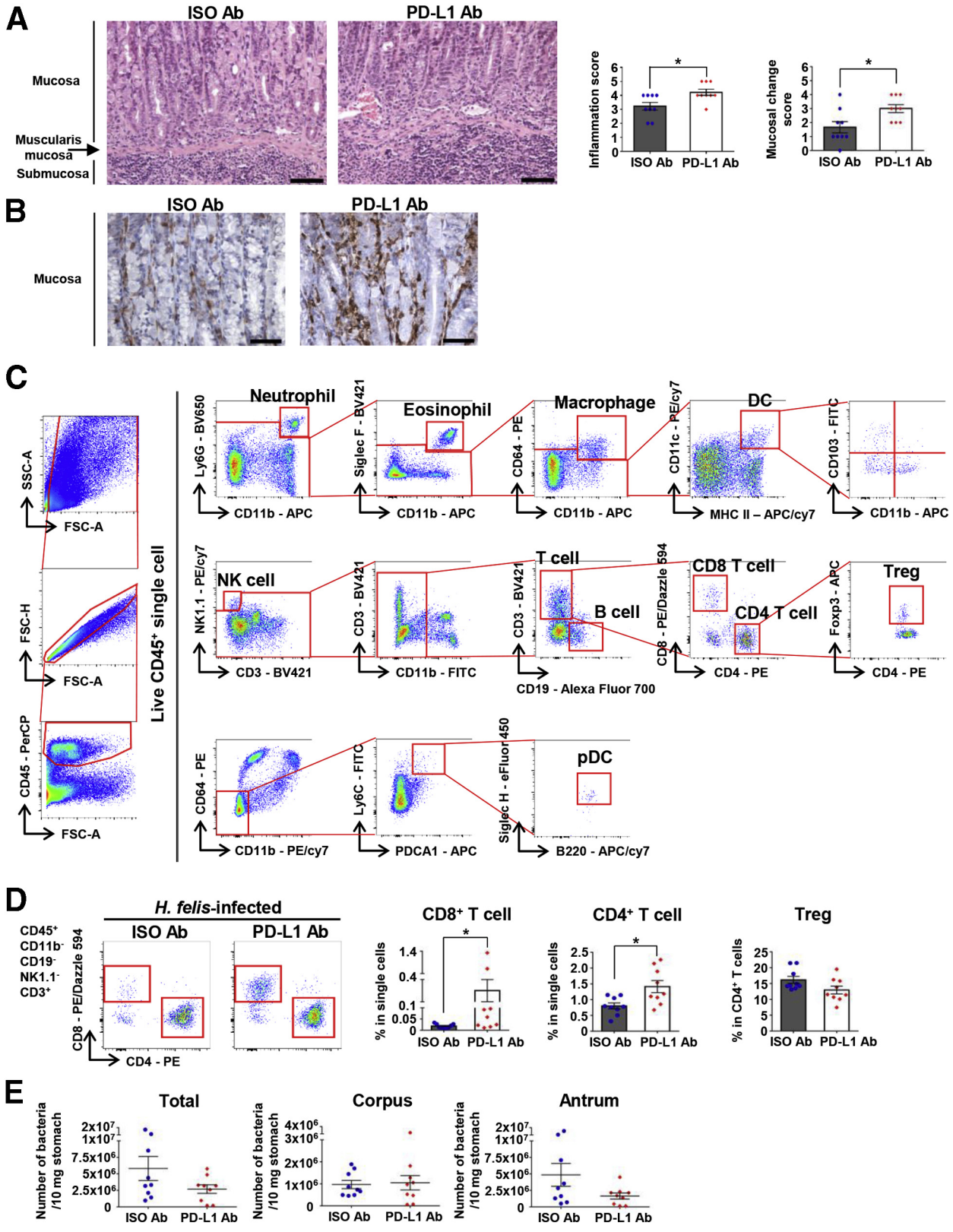

more severe in the *Pdl1*$^{-/-}$ BM transplanted (BMT) mice compared with control mice (Figure 2*A*). The inflammatory processes induced by *Helicobacter* infection can damage the mucosa, causing oxyntic atrophy and precancerous mucosal metaplasia. In the corpus mucosa of *H felis*–infected mice, varying numbers of parietal cells and mature chief cells were lost and replaced by mucous cells showing spasmolytic polypeptide-expressing metaplasia (SPEM). In addition, foveolar cell hyperplasia was observed. We confirmed the loss of parietal cells using immunohistochemistry (IHC) for H^+/K^+-adenosine triphosphatase (ATPase) and the degree of mucous neck cell hyperplasia and SPEM using Alcian blue staining. In the *Pdl1*$^{-/-}$ BMT mice, parietal cell loss worsened, and Alcian blue positive cells were more prominent (Figure 2*B*). Accumulation of T cells and neutrophils, but not macrophages, was more severe in the *Pdl1*$^{-/-}$ BMT mice than in control mice. However, the percentage of Tregs in $CD4^+$ T cells tended to be lower in the *Pdl1*$^{-/-}$ BMT mice than those in control mice (Figure 2*C*). Bacterial load in the stomach was decreased markedly in *Pdl1*$^{-/-}$ BMT mice than in control mice (Figure 2*D*).

CD11c$^+$ *Cells Mainly Express PD-L1 and Co-localize With PD-1–Expressing T Cells in* Helicobacter*-Infected Gastric Mucosa and Submucosa*

To analyze the pattern of PD-L1 expression in *Helicobacter*-infected gastric tissue, we performed immunofluorescence staining for PD-L1, CD45, CD3, CD11c, and PD-1 in *H felis*–infected gastric tissue. PD-$L1^+$ cells were located mainly in the submucosa and mucosal laminar propria immediately above the muscularis mucosa. However, mucosal epithelial cells showed scant PD-L1 expression (Figure 3*A* and *B*). The majority of PD-$L1^+$ cells co-stained with CD45 (Figure 3*A*), and these $CD45^+$PD-$L1^+$ cells were in contact with $CD3^+$ cells (Figure 3*B*). In addition, $CD11c^+$ cells expressed PD-L1, and the majority of $CD3^+$ cells expressed PD-1 (Figure 3*C*). These results indicate that PD-L1–expressing $CD11c^+$ cells interact with PD-1^+CD3^+ T cells in the *H felis*–infected gastric mucosa and submucosa.

Gastric cDCs Express a High Level of PD-L1

To further characterize PD-L1 expression in gastric CD11c-positive cells, we performed flow cytometry analysis on gastric immune cells. First, we gated out $CD45^+$ leukocytes from the live cell population and then sequentially excluded neutrophils ($Ly6G^+CD11b^+$), eosinophils (Siglec F^+CD11b^+), and macrophages ($CD64^+CD11b^+$) from the $CD45^+$ cells. Next, we defined $CD11c^+$Major histocompatibility complex class II (MHC II)$^+$ cells and further analyzed their CD103 and CD11b expression (Figure 4*A* and *B*). To confirm that these gastric $CD11c^+$MHC II^+ subsets were bona fide DCs, we analyzed the expression level of Zinc finger and BTB domain containing 46 (ZBTB46), a marker of human and murine DCs,[24,25] in *H felis*–infected WT mice. As expected, gastric macrophages, neutrophils, and eosinophils did not express ZBTB46, while gastric $CD11c^+$MHC II^+ cells expressed high levels (Figure 4*A*). Furthermore, a t-stochastic neighborhood embedding algorithm was used to perform dimensionality reduction and visualization of DC subpopulations stained with CD45, CD11c, MHC II, Siglec F, Ly6G, CD64, CD11b, CD103, Interferon regulatory factor 4 (IRF4), Interferon regulatory factor 8 (IRF8), Signal regulatory protein alpha (SIRPα), CD24, and X-C motif chemokine receptor 1 (XCR1) antibodies. We found that gastric DCs can be divided into 2 populations containing $CD103^+CD11b^-$ DCs—a part of double-negative (DN) DCs and $CD103^-CD11b^+$ DCs—the other half of DN DCs (Figure 4*B*). From the flow cytometry analysis, we defined $CD103^+CD11b^-$ DCs as cDC1: $IRF4^-IRF8^+SIRP\alpha^-CD24^{high}XCR1^{high}$, and $CD103^-CD11b^+$ DCs as cDC2: $IRF4^+IRF8^-SIRP\alpha^+CD24^{low}XCR1^{low}$. The DN subset, $CD103^-CD11b^-$ DCs contained 2 populations: cDC1 and cDC2-like DCs (Figure 4*B* and *C*). These cDC populations also were well-conserved in normal gastric tissue (Figure 4*D*). Similar $CD103^-CD11b^-$ DN DCs also were identified in the heart, lung, and liver, and even in solid tumors, and were assumed to represent an intermediate stage of cDC maturation.[26,27]

Next, we examined the expression level of PD-L1, PD-L2, and T-cell co-stimulatory molecules, including CD80, CD86, and CD40, on innate immune cells. Regardless of *H felis* infection, all gastric DC subsets expressed higher levels of PD-L1 than those of other gastric immune cells, including macrophages and neutrophils. Although *H felis* infection did not affect the PD-L1 expression level on individual gastric DCs regardless of the DC subsets, *H felis* infection did increase the number of PD-L1–expressing gastric DCs, resulting in an increase in the total level of PD-L1 expression (Figure 4*E*). To confirm whether similar results were observed in *H pylori* infection as in *H felis* infection, we infected mice with *H pylori* Sydney strain 1 containing virulence factors Cytotoxin-associated gene A (CagA) and Vacuolating cytotoxin A (VacA), and analyzed the results 18 months later. *H pylori* infection increased PD-L1 expression on gastric DCs, which also was significantly higher than on macrophages. In particular, PD-L1

Figure 1. (***See previous page***). **Blockade of PD-L1 enhances gastric inflammation upon *H felis* infection for 4 weeks.** (*A*) Histopathologic analysis of *H felis*–induced gastritis, oxyntic atrophy, and mucosal metaplasia according to grading criteria on H&E stain. Representative H&E images of the gastric corpus regions of isotype control mice and mice with PD-L1 blockade (*left*). Inflammation score and mucosal change score (*right*) (isotype control mice, n = 9; PD-L1 blockade mice, n = 9). *Scale bar*: 100 μm. (*B*) More severe mucosal infiltration of T cells in the gastric corpus regions of mice with PD-L1 blockade. Representative images of CD3 IHC (3,3'-diaminobenzidine substrate). *Scale bar*: 50 μm. (*C*) Gating strategy for the analysis of gastric immune cells. (*D*) Percentage of $CD8^+$ T cells and $CD4^+$ T cells in live single cells and of Tregs in live $CD4^+$ T cells from the stomach of mice with PD-L1 blockade (n = 9) and isotype control mice (n = 9). Representative flow cytometry plots (*left*). (*E*) The bacterial loads were evaluated using quantitative real-time PCR for *H felis* flagellar filament B DNA extracted from the corpus and antrum, respectively (isotype control mice, n = 9; PD-L1 blockade mice, n = 9). Data are presented as means ± SEM. **P* < .05. APC, allophycocyanin; FITC, fluorescein isothiocyanate; FSC, forward scatter; ISO, isotype control; NK, natural killer; PE, phycoerythrin; SSC, side scatter.

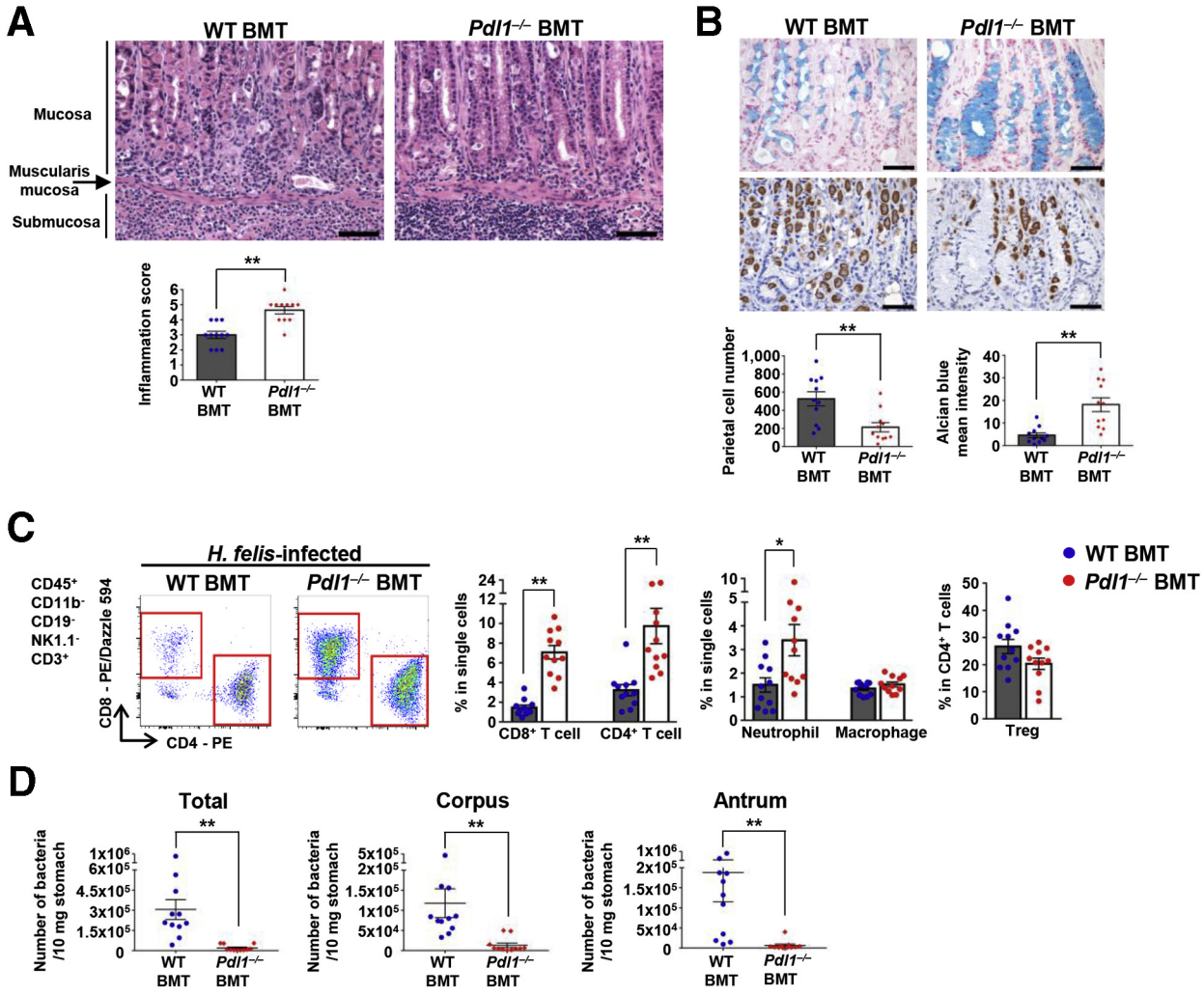

Figure 2. PD-L1 deficiency in BM-derived cells enhances gastric inflammation with mucosal metaplasia upon *H felis* infection for 4 weeks. (*A*) Histopathologic analysis of *H felis*–induced gastritis. Representative H&E images of the gastric corpus regions of WT BMT and *Pdl1*$^{-/-}$ BMT mice (*top*). Inflammation score (*bottom*) (WT BMT, n = 11; *Pdl1*$^{-/-}$ BMT, n = 11). *Scale bar*: 100 μm. (*B*) Histopathologic analysis of *H felis*–induced oxyntic atrophy and mucosal metaplasia. Representative serial images of the gastric corpus regions of WT BMT (*left*) and *Pdl1*$^{-/-}$ BMT (*right*) mice after Alcian blue staining (*top*) and H^+/K^+-ATPase IHC (*bottom*). Quantification of H^+/K^+-ATPase$^+$ cells (parietal cells) and Alcian blue–positive region (WT BMT, n = 11; *Pdl1*$^{-/-}$ BMT, n = 11). *Scale bar*: 50 μm. (*C*) Percentage of CD8$^+$ T cells, CD4$^+$ T cells, neutrophils, and macrophages in live single cells and of Tregs in live CD4$^+$ T cells from the stomach of WT BMT (n = 11) and *Pdl1*$^{-/-}$ BMT (n = 11) mice. Representative flow cytometry plots of T cells (*left*). (*D*) *H felis* loads were evaluated using quantitative real-time PCR for *H felis* flagellar filament B DNA extracted from the corpus and antrum, respectively (WT BMT, n = 11; *Pdl1*$^{-/-}$ BMT, n = 11). Data are presented as means ± SEM. **P* < .05 and ***P* < .01. PE, phycoerythrin.

expression on the CD11b$^+$ DC subset was increased markedly by *H pylori* infection (Figure 4*F*). Gastric DCs also expressed higher levels of PD-L1 than splenic DCs upon *H felis* infection (Figure 4*G*). The CD80 expression level of gastric DCs, excluding CD103$^+$ DCs, was not affected by *H felis* infection, whereas that of CD103$^+$ DCs was decreased during *H felis* infection. In addition, the CD86 expression level of all gastric DC subsets was decreased during *H felis* infection. However, compared with the median fluorescence intensity of isotype control, CD40 or PD-L2 in gastric DCs and DC subsets showed scant expression, regardless of *H felis* infection (Figure 5*A*). A similar PD-L2 expression pattern of gastric DCs was observed in *H pylori* infection (Figure 5*B*).

Helicobacter *Infection Increases DCs in Gastric Mucosa and Submucosa*

To confirm the location of DCs in the normal mouse stomach, we performed immunostaining for CD11c and observed the stomach of normal CD11c–Enhanced Yellow Fluorescent Protein (EYFP) mice using confocal microscopy. CD11c$^+$ cells were very few and were located mainly in the superficial mucosal lamina propria and around the limiting ridge (Figure 6*A*). In contrast, during *H felis* infection, CD11c$^+$ cells were located mainly in the inflamed submucosa and mucosal laminar propria immediately above the muscularis mucosa. A few cells also were distributed throughout the mucosal lamina propria. The number of

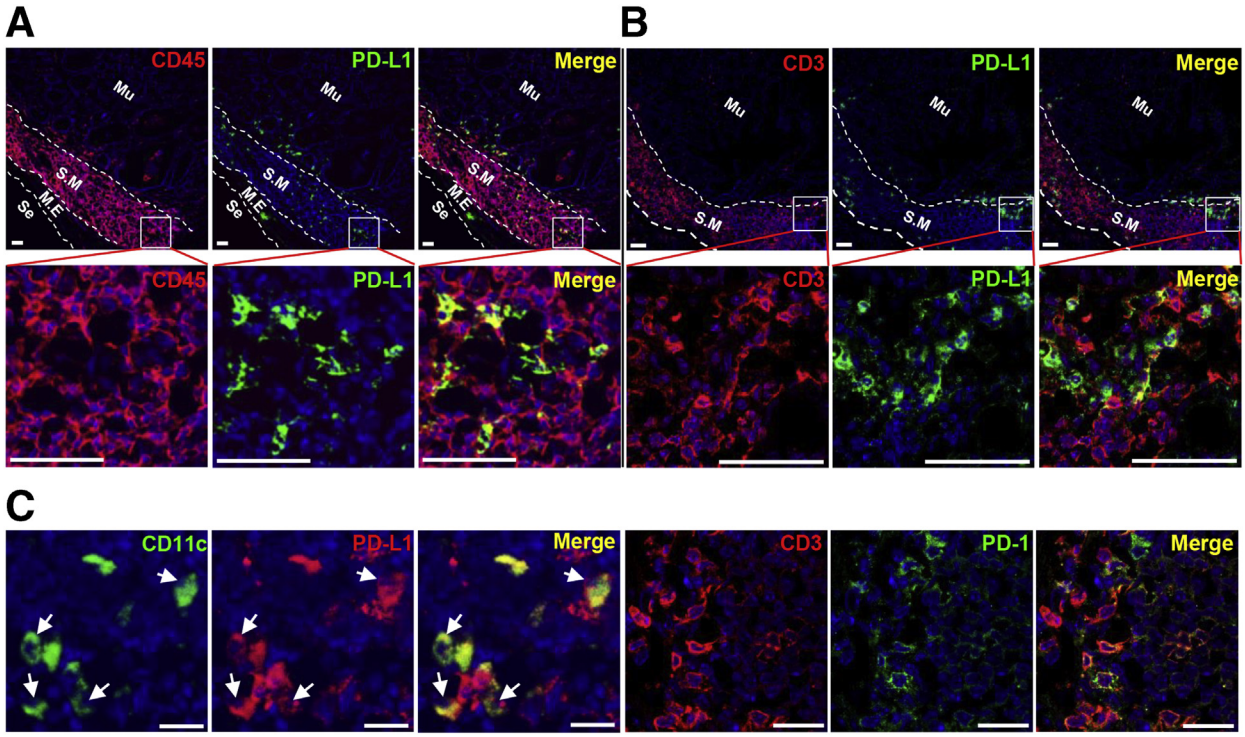

Figure 3. Location of PD-L1–expressing immune cells in the stomach during *Helicobacter* infection. (*A–C*) Immunofluorescence for PD-L1, CD45, CD3, CD11c, and PD-1 in the gastric corpus regions of *H felis*–infected WT mice. (*A* and *B*) Note the localization of PD-L1$^+$ cells in the submucosa and mucosal laminar propria immediately above the muscularis mucosa. PD-L1$^+$ cells are co-stained with CD45 and co-localize with CD3$^+$ T cells. *Scale bar*: 50 μm. (*C*) PD-L1$^+$CD11c$^+$ cells (*arrows*) and PD-1$^+$CD3$^+$ T cells in the submucosa. *Scale bar*: 20 μm. M.E, muscularis externa; Mu, mucosa; Se, serosa; S.M, submucosa.

CD11c$^+$ cells infiltrating the stomach gradually increased at 2, 4, and 8 weeks of *H felis* infection (Figure 6*B*). Under normal conditions, gastric CD11c$^+$MHC II$^+$ cells comprised approximately 0.24% of the total live cells and were composed of 3 subsets, CD103$^+$CD11b$^-$ (17.9%), CD103$^-$CD11b$^+$ (45.3%), and CD103$^-$CD11b$^-$ (DN; 32.1%) populations (Figure 6*C*). During *H felis* infection, infiltration of leukocytes and DCs into the stomach was increased markedly. All subsets of CD11c$^+$MHC II$^+$ cells gradually increased at 2, 4, and 8 weeks of *H felis* infection (Figure 6*C*).

Flt3$^{-/-}$ *Mice Showed Decreased Number of Gastric DCs and Developed Severe Gastric Inflammation With Less* Helicobacter *Colonization*

To determine the role of DCs in *Helicobacter*-induced gastritis, we investigated whether the immune response differed between *H felis*–infected fms-like tyrosine kinase 3 (Flt3) knockout (*Flt3*$^{-/-}$) and WT mice. The receptor tyrosine kinase Flt3 is an important regulator of DC homeostasis at the periphery, and cDCs and plasmacytoid DCs (pDCs) are depleted in the peripheral lymphoid and nonlymphoid tissues by Flt3 deficiency.[28–30] We confirmed that the number of total DCs and DC subsets, including CD103$^+$, CD11b$^+$, and DN DCs, but not macrophages, was markedly lower in the stomach of *Flt3*$^{-/-}$ mice than in WT mice (Figure 7*A*). Next, we compared the severity of gastritis between the 2 groups at 2, 4, and 8 weeks after *H felis* infection. Histologically, inflammation occurred mainly in the corpus. In WT mice, neutrophil infiltration into the submucosa was observed mainly after 2 weeks of infection, and lymphocyte and plasma cell infiltration was noted at 4 weeks, and most prominently at 8 weeks after infection. These inflammatory cells mostly infiltrated the submucosa, and as the severity of gastritis increased, infiltrated the mucosal lamina propria. In addition, lymphoid follicles occasionally were present in the submucosa or mucosa. In contrast, in *Flt3*$^{-/-}$ mice, infiltration of not only neutrophils but also many lymphocytes and plasma cells was noted at 2 weeks and continued to increase gradually until 8 weeks. Infiltration of inflammatory cells was observed mainly in the submucosa, but often diffusely expanded into the entire mucosal lamina propria, showing that *Flt3*$^{-/-}$ mice had more severe gastric inflammation compared with WT controls (Figure 7*B*). PD-L1 messenger RNA (mRNA) expression in gastric tissue was decreased significantly in *Flt3*$^{-/-}$ mice than in WT mice during *H felis* infection (Figure 7*C*).

H felis was mainly present in the lumen of the gastric pits and mucus layer throughout the glandular region (Figure 7*D*). The extent of *H felis* colonization in WT mice tended to increase gradually during 8 weeks of infection, although not in *Flt3*$^{-/-}$ mice. In particular, at 8 weeks after *H felis* infection, the extent of *H felis* colonization was lowest in

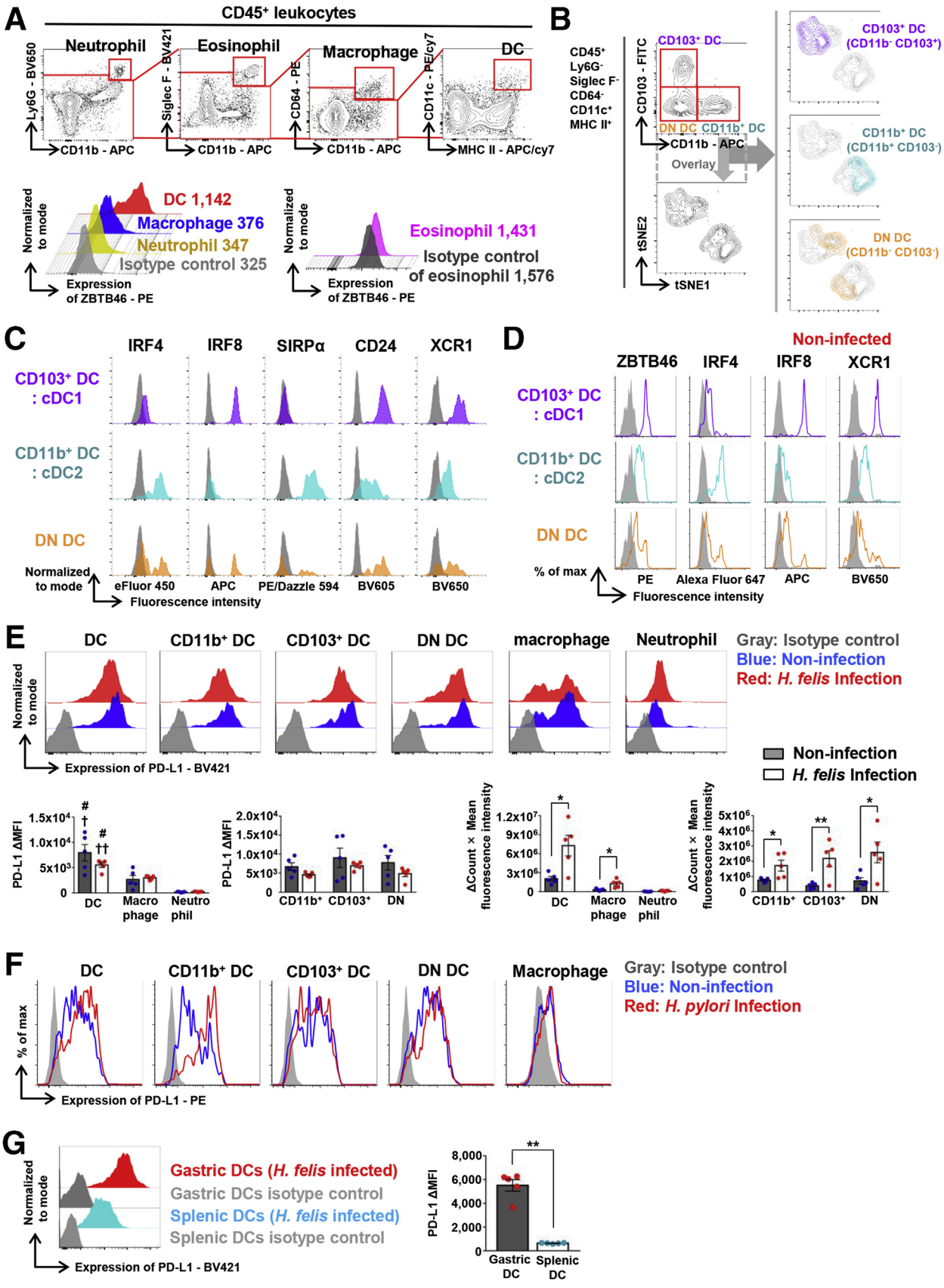
A
CD45+ leukocytes
Neutrophil
Eosinophil
Macrophage
DC
Ly6G - BV650
Siglec F - BV421
CD64 - PE
CD11c - PE/cy7
CD11b - APC
MHC II - APC/cy7
Normalized to mode
DC 1,142
Macrophage 376
Neutrophil 347
Isotype control 325
Expression of ZBTB46 - PE
Eosinophil 1,431
Isotype control of eosinophil 1,576
B
CD45+ Ly6G- Siglec F- CD64- CD11c+ MHC II+
CD103+ DC
DN DC
CD11b+ DC
CD103 - FITC
CD11b - APC
Overlay
tSNE2
tSNE1
CD103+ DC (CD11b- CD103+)
CD11b+ DC (CD11b+ CD103-)
DN DC (CD11b- CD103-)
C
IRF4
IRF8
SIRPα
CD24
XCR1
CD103+ DC : cDC1
CD11b+ DC : cDC2
DN DC
Normalized to mode
eFluor 450
APC
PE/Dazzle 594
BV605
BV650
Fluorescence intensity
D
Non-infected
ZBTB46
IRF4
IRF8
XCR1
% of max
PE
Alexa Fluor 647
APC
BV650
E
DC
CD11b+ DC
CD103+ DC
DN DC
macrophage
Neutrophil
Gray: Isotype control
Blue: Non-infection
Red: H. felis Infection
Expression of PD-L1 - BV421
Non-infection
H. felis Infection
PD-L1 ΔMFI
ΔCount × Mean fluorescence intensity
Macro phage
Neutro phil
F
DC
CD11b+ DC
CD103+ DC
DN DC
Macrophage
Gray: Isotype control
Blue: Non-infection
Red: H. pylori Infection
% of max
Expression of PD-L1 - PE
G
Gastric DCs (H. felis infected)
Gastric DCs isotype control
Splenic DCs (H. felis infected)
Splenic DCs isotype control
Normalized to mode
Expression of PD-L1 - BV421
PD-L1 ΔMFI
Gastric DC
Splenic DC

the mucosa of *Flt3*$^{-/-}$ mice. Overall, the bacterial load was lower in *Flt3*$^{-/-}$ mice than in WT mice, and this difference was most noticeable after 8 weeks of infection (Figure 7*D* and *E*). *Helicobacter* colonization can be affected by various microenvironmental factors in gastric tissue. Previous studies have shown a positive correlation between the degree of gastritis and clearance of *Helicobacter*.[19,31] In addition, surfactant protein-D (SP-D) has been reported to play a crucial role in the elimination of *Helicobacter* from the luminal mucus layer.[32–34] In this study, the level of SP-D was increased during *H felis* infection and was much higher in *H felis*–infected *Flt3*$^{-/-}$ mice than in *H felis*–infected WT mice (Figure 7*F*). Therefore, the increased gastric inflammation and SP-D accumulation may be associated with high clearance of *H felis* in *Flt3*$^{-/-}$ mice.

Flt3$^{-/-}$ *Mice Have Enhanced Mucosal Metaplasia Upon* Helicobacter *Infection*

Because *H felis*–infected *Flt3*$^{-/-}$ mice showed profound inflammation in gastric mucosa, we further characterized precancerous changes including loss of parietal cells, mucous neck cell hyperplasia, and SPEM (Figure 8). Trefoil factor 2 (TFF2) is a marker of mucous neck cells and SPEM,[35] and Clusterin (CLU) expression increases as SPEM progresses.[36,37] In our results, as the duration of *H felis* infection progressed, parietal cell loss worsened, and Alcian blue–positive cells were seen to replace the lost parietal cells. The pattern of TFF2 and CLU expression was relatively similar to that of Alcian blue staining. TFF2 and CLU expression was observed in a few cells in the isthmus regions of the gastric mucosa in normal WT mice, whereas in *H felis*–infected mice, it was observed mainly at the base regions of the mucosa or throughout the mucosa. In particular, the areas of Alcian blue–, TFF2-, and CLU-positive mucosa in *H felis*–infected *Flt3*$^{-/-}$ mice were more prominent than in *H felis*–infected WT mice (Figure 8). Some of these metaplastic mucosal cells showed proliferative behavior according to Ki67 staining, and the number of Ki67-positive cells in the base regions of the mucosa was higher in *H felis*–infected *Flt3*$^{-/-}$ mice than in *H felis*–infected WT mice (Figure 8*B* and *C*).

Flt3$^{-/-}$ *Mice Showed More Prominent CD8*$^{+}$ *T-Cell Accumulation Upon* Helicobacter *Infection*

Among the various leukocyte populations that infiltrated the *H felis*–infected stomach, T-cell infiltration was the most prominent difference between WT and *Flt3*$^{-/-}$ mice. In *Flt3*$^{-/-}$ mice, infiltration of CD8^{+} T cells was dramatically higher than in WT mice, and infiltration of CD4^{+} T cells also tended to be greater in *Flt3*$^{-/-}$ mice than in WT mice when the *H felis* infection persisted for 8 weeks. In addition, in *Flt3*$^{-/-}$ mice compared with WT mice, neutrophil infiltration was more pronounced 2 weeks after *H felis* infection, and also tended to be more pronounced 8 weeks after *H felis* infection. However, no difference in the extent of macrophage infiltration was noted between the 2 groups. On the other hand, the percentage of Tregs in CD4^{+} T cells was reduced significantly in *Flt3*$^{-/-}$ mice compared with that in WT mice 8 weeks after *H felis* infection (Figure 9*A*). These phenotypes were recapitulated in the *H pylori*–infected *Flt3*$^{-/-}$ mice (Figure 9*B*). Furthermore, in *H pylori* infection, gastritis tended to be more severe in *Flt3*$^{-/-}$ mice than in WT mice. According to the histopathologic grading criteria, inflammation scores were 2 ± 1 in *Flt3*$^{-/-}$ mice and 1 or 2 in WT mice (Figure 9*C*). T-cell infiltration was more prominent not only in the submucosa but also in the mucosal lamina propria in *H felis*–infected *Flt3*$^{-/-}$ mice than in *H felis*–infected WT mice (Figure 9*D*). However, the number of splenic T cells was not different between the 2 groups (Figure 9*E*). *H felis* infection increased the mRNA expression of various factors related to inflammation. Expression of IFN-γ was approximately 6-fold higher in *H felis*–infected *Flt3*$^{-/-}$ mice than in *H felis*–infected WT mice. In addition, granzyme A and perforin were approximately 2.9- and 2.2-fold higher in *Flt3*$^{-/-}$ mice than in WT mice, respectively (Figure 9*F*). Levels of various chemokines, including CCL2 (monocyte chemoattractant protein-1), CCL3 (macrophage inflammatory protein-1α), CCL4 (macrophage inflammatory protein-1β), CCL5 (regulated on activation, normal T cell expressed and secreted), and CCL8 (monocyte chemoattractant protein-2), were higher in the gastric tissue of *H felis*–infected *Flt3*$^{-/-}$ mice than in *H felis*–infected WT mice. The difference between the 2 groups was clearly observed

Figure 4. (***See previous page***). **Gastric cDCs express a high level of PD-L1.** (*A*) Gating strategy of DCs, defined as CD45^{+}Ly6G^{-}Siglec F^{-}CD64^{-}CD11c^{+}MHC II^{+} cells and expression of ZBTB46 in gastric DCs, macrophages, neutrophils, and eosinophils. Numbers in the histogram represent the median fluorescence intensity of ZBTB46 in each population. Note that DCs express considerably higher levels of ZBTB46 than other cell types. (*B*) A t-stochastic neighborhood embedding (tSNE) plot of total gastric cDCs and overlay of each cDC subset. (*C*) Expression of IRF4, IRF8, SIRPα, CD24, and XCR1 in 3 gastric cDC subsets under *H felis* infection. (*D*) Expression of ZBTB46, IRF4, IRF8, and XCR1 in 3 gastric cDC subsets under normal conditions. Gray indicates isotype control. (*A–D*) Concatenated data from 3 independent experiments. (*E*) PD-L1 expression on innate immune cells 8 weeks after *H felis* infection. Δ mean fluorescence intensity (MFI) = (sample MFI) – (isotype control MFI) Δ(count × MFI) = ([count × mean fluorescence intensity] of sample) – ([count × mean fluorescence intensity] of isotype control). Note that DCs and DC subsets express considerably higher levels of PD-L1 than other cell types. Each figure represents 5 independent experiments. Three mice per group were pooled for each experiment. Data are presented as means ± SEM. $^{\dagger}P < .05$, and $^{\dagger\dagger}P < .01$, compared with macrophages; $^{\#}P < .01$, compared with neutrophils; $^{*}P < .05$ and $^{**}P < .01$, compared between the noninfected and *H felis*–infected groups. (*F*) As in panel *E*, but with *H pylori* infection. Note that DCs and DC subsets express considerably higher levels of PD-L1 than macrophages. (*G*) Comparison of PD-L1 expression levels in gastric DCs and splenic DCs 8 weeks after *H felis* infection. The left figure is representative of the 5 experiments. ΔMFI = (sample MFI) – (isotype control MFI). Three mice per group were pooled for each experiment. Stomach and spleen were collected from the same individuals. Data are presented as means ± SEM. $^{**}P < .01$. APC, allophycocyanin; FITC, fluorescein isothiocyanate.

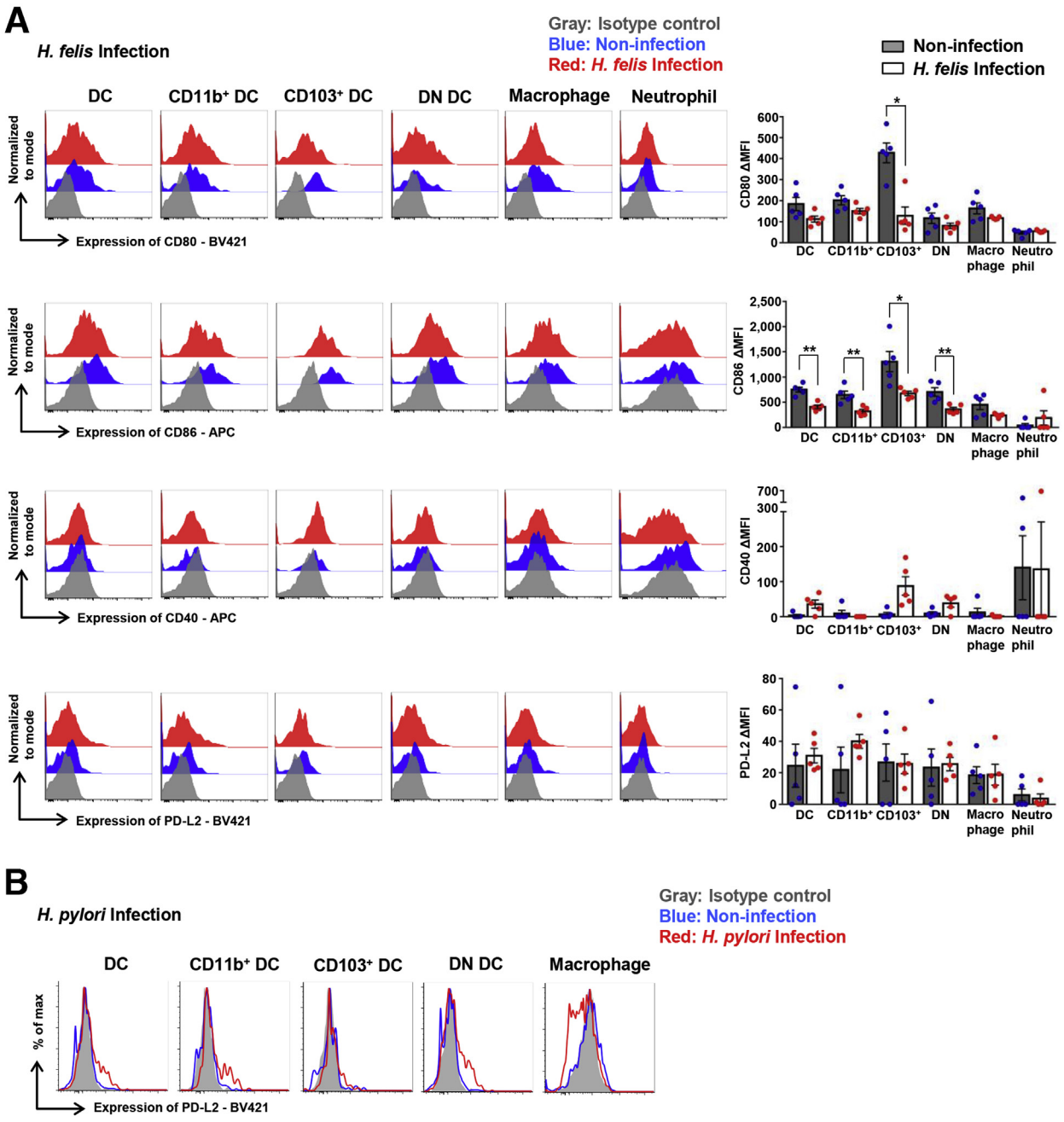

Figure 5. Expression level of co-stimulatory molecules and PD-L2 in gastric DCs. (*A*) Expression levels of CD80, CD86, CD40, and PD-L2 on innate immune cells 8 weeks after *H felis* infection. Data are presented as means ± SEM. **P* < .05 and ***P* < .01. Each figure is representative of 5 independent experiments. Three mice per group were pooled for each experiment. (*B*) Expression level of PD-L2 on innate immune cells 18 months after *H pylori* infection. Three mice per group were pooled for the experiment. APC, allophycocyanin; max., maximum.

after 8 weeks of *H felis* infection (Figure 9*G*). These chemokines can contribute to T-cell migration into the peripheral site of infection,[38,39] supporting enhanced $CD8^+$ T-cell accumulation in gastric tissues in DC ablated mice. To confirm that the enhanced gastritis in $Flt3^{-/-}$ mice was driven by hematopoietic FLT3 deficiency, lethally irradiated WT mice were transplanted with $Flt3^{-/-}$ BM or WT BM as control. The *H felis*–infected recipient mice were analyzed 8 weeks after infection. Flow cytometry analysis of the gastric tissues showed that all subsets of gastric DCs were decreased significantly in $Flt3^{-/-}$ BMT mice compared with those in WT BMT mice (Figure 10*A*). Although the difference was not statistically significant, PD-L1 mRNA expression in gastric tissue tended to decrease in $Flt3^{-/-}$ BMT mice compared with that in WT BMT mice during *H felis* infection (Figure 10*B*) ($P = .0927$). $CD8^+$ and $CD4^+$ T-cell accumulation was more prominent in $Flt3^{-/-}$ BMT mice than that in WT BMT mice. The percentage of Tregs in $CD4^+$ T cells tended to be lower in

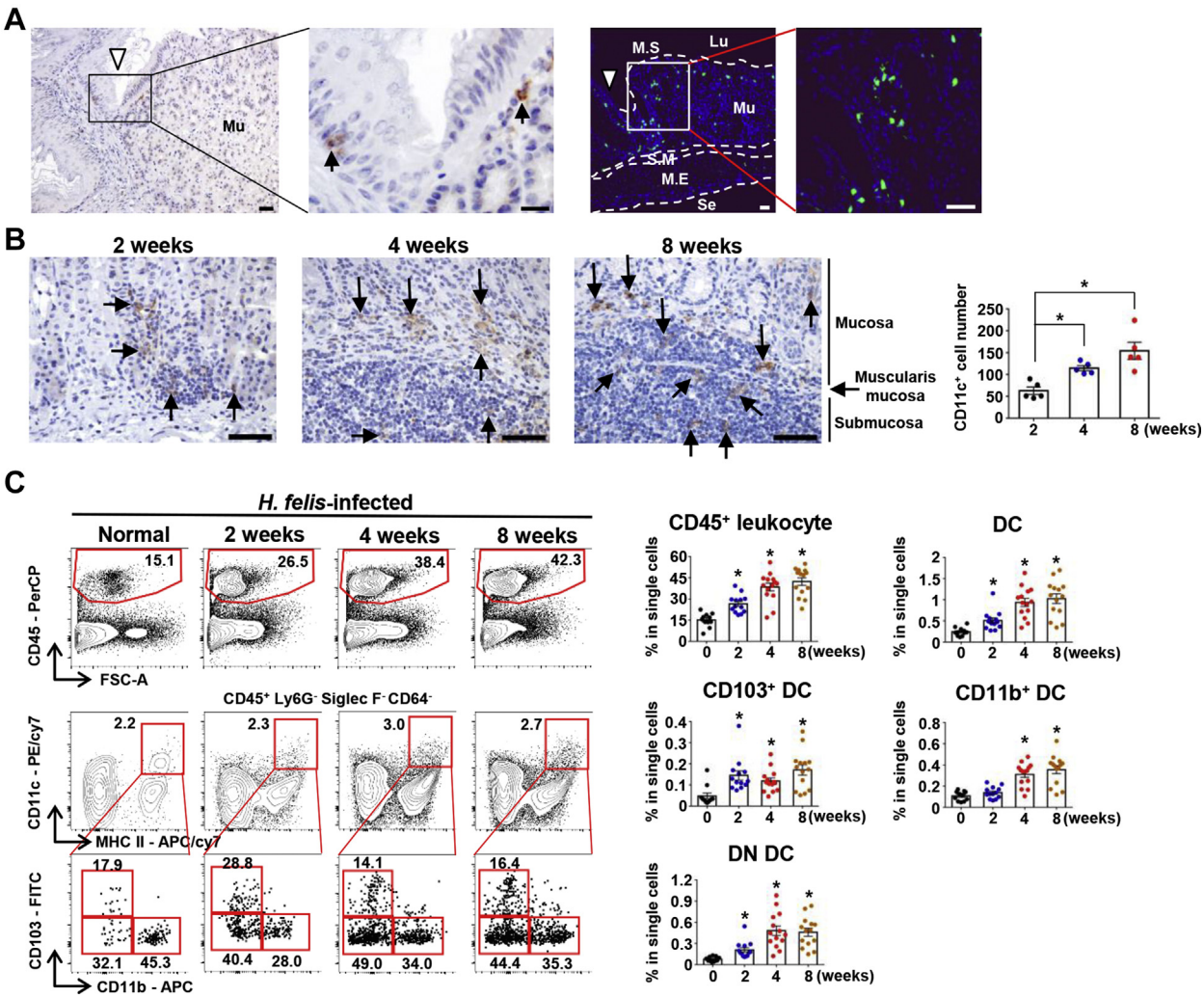

Figure 6. *Helicobacter* infection increases DCs in gastric mucosa and submucosa. (*A*) Localization of CD11c$^+$ DCs (*arrows*) under steady state. *Left*: Representative images of CD11c IHC (3,3'-diaminobenzidine substrate). *Right*: Representative images of normal CD11c-Enhanced Yellow Fluorescent Protein (EYFP) mouse stomach. *White arrowhead* indicates a limiting ridge at the boundary of the glandular and nonglandular stomach. *Scale bar*: 50 μm. (*B*) Localization and number of gastric CD11c$^+$ DCs (*arrows*) in the gastric corpus regions of *H felis*–infected WT mice. *Left*: Representative images of CD11c IHC (3,3'-diaminobenzidine substrate). *Right*: Manual cell count of CD11c$^+$ DCs in 2 paraffin sections (n = 5 for each group). *Scale bar*: 50 μm. (*C*) Numeric increase in gastric DCs during *H felis* infection. Percentage of leukocytes, DCs, and DC subsets in live single cells from the stomach of WT mice with *H felis* infection. *Left*: Representative flow cytometry plots. *Right*: Asterisks at 2, 4, and 8 weeks after *H felis* infection (n = 13–14 for each group) signify a significant increase compared with that in normal WT mice (n = 11). Data are presented as means ± SEM. *$P < .01$. Week, duration of infection. APC, allophycocyanin; FITC, fluorescein isothiocyanate; FSC, forward scatter; Lu, lumen; M.E, muscularis externa; Mu, mucosa; M.S, mucosal surface; PerCP, peridinin-chlorophyll-protein complex; Se, serosa.

Flt3$^{-/-}$ BMT mice than that in WT BMT mice (Figure 10*C*). The bacterial load in the stomach was lower in *Flt3*$^{-/-}$ BMT mice than that in WT BMT mice (Figure 10*D*).

Depletion of cDCs Enhanced Helicobacter*-Induced Gastric Inflammation*

Because *Flt3*$^{-/-}$ mice lack pDCs as well as cDCs, we could not rule out the involvement of pDCs in the suppression of T-cell response to *H felis*. Therefore, we attempted to dissect the function of *Flt3*-dependent cDCs and pDCs in *Helicobacter* infection using *Zbtb46*-diphtheria toxin receptor (DTR) and *BDCA2*-DTR mice. Lethally irradiated mice were transplanted with BM from *Zbtb46*-DTR or *BDCA2*-DTR mice. We analyzed gastric lesions 4 weeks after *H felis* infection. Gastric DCs were effectively ablated by diphtheria toxin (DT) injection in *Zbtb46*-DTR BMT mice (Figure 11*A*). Both CD4$^+$ T-cell and CD8$^+$ T-cell accumulation was increased markedly in cDC-ablated mice. In addition, infiltration of neutrophils and macrophages also was increased significantly in cDC-ablated mice. However, the percentage of Tregs in CD4$^+$ T cells was reduced significantly by cDC depletion (Figure 11*B*). Histologically, cDC ablation resulted in more severe inflammation and pathologic mucosal changes (Figure 11*C*–*E*). Expression of IFN-γ mRNA in gastric tissues was increased markedly in cDC-ablated mice (Figure 11*F*). Although there was no

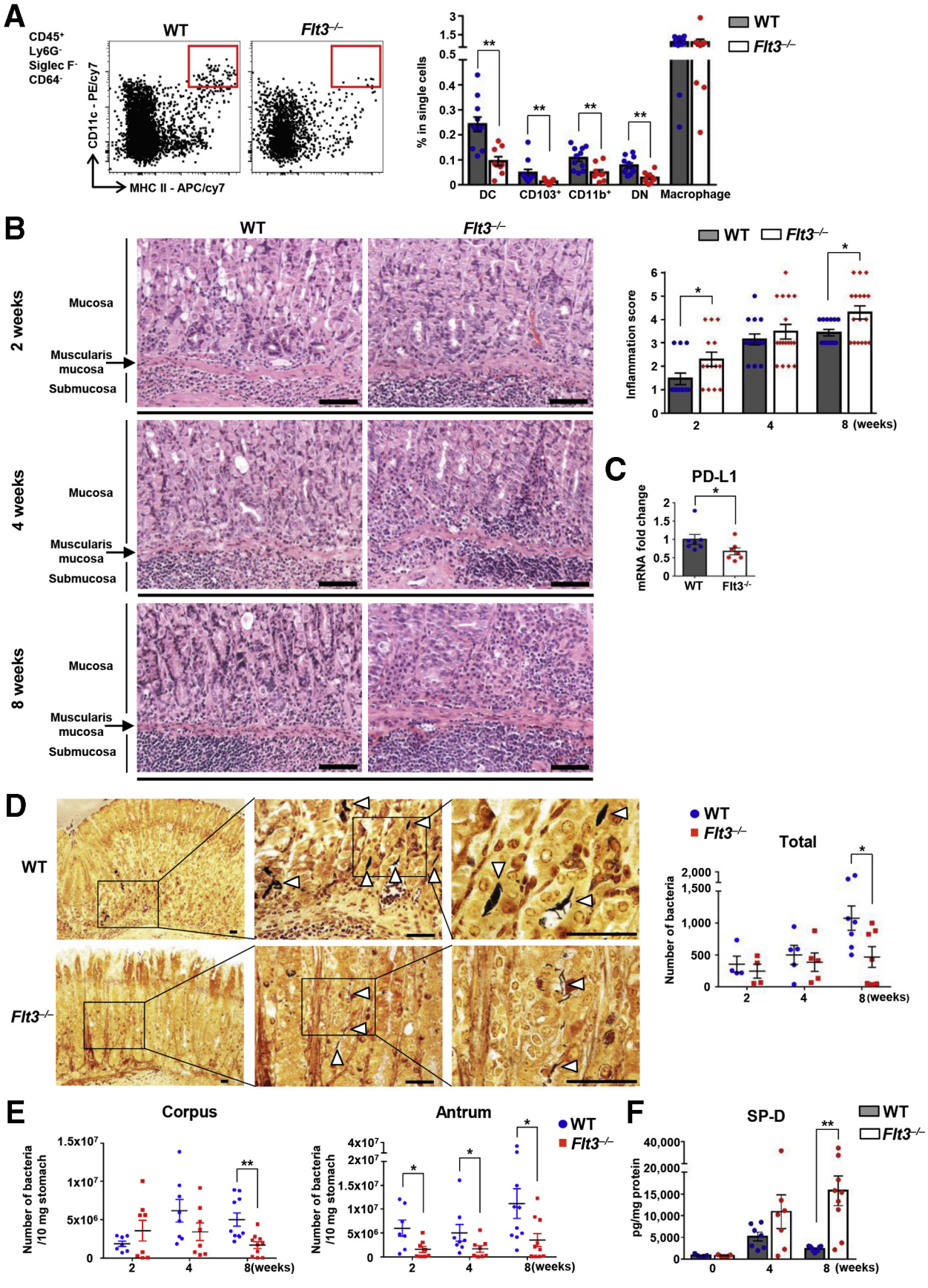
A
CD45+
Ly6G-
Siglec F-
CD64-
WT
Flt3−/−
CD11c - PE/cy7
MHC II - APC/cy7
% in single cells
DC
CD103+
CD11b+
DN
Macrophage
B
2 weeks
4 weeks
8 weeks
Mucosa
Muscularis mucosa
Submucosa
Inflammation score
8 (weeks)
C
PD-L1
mRNA fold change
Flt3-/-
D
Total
Number of bacteria
E
Corpus
Antrum
Number of bacteria /10 mg stomach
F
SP-D
pg/mg protein

statistical significance, the bacterial loads in the stomach tended to decrease in cDC-ablated mice compared with those in control mice (Figure 11*G*).

Gastric pDCs were identified as a $CD64^{-}CD11b^{-}Ly6\text{-}C^{hi}PDCA1^{+}B220^{+}$Siglec H^{+} population (Figure 1*C*). DT injection into *BDCA2*-DTR BMT mice effectively eliminated pDCs, but did not affect cDCs (Figure 11*H*). However, no differences in T-cell accumulation in the stomach were noted between pDC-ablated mice and control mice during *H felis* infection (Figure 11*I*). The bacterial loads in the stomach were not changed in pDC-ablated mice (Figure 11*J*). Taken together, these results indicate that gastric cDCs, but not pDCs, control gastric T-cell populations during *Helicobacter* infection.

PD-L1–Expressing DCs Co-localized With T Cells in Human Helicobacter*-Positive Gastritis*

To determine whether PD-L1–expressing DCs co-localize with T cells in the gastric tissue of *H pylori*–infected patients, we performed multiplexed IHC for CD11c, PD-L1, and CD3. $CD11c^{+}$ cells were distributed in the mucosal lamina propria and submucosa, and their numbers were significantly higher in the stomach of *H pylori*–positive patients and patients with mucosal dysplasia than in *H pylori*–negative patients. PD-L1 expression was found mostly in infiltrated cells, and not in epithelial cells. Importantly, the $CD11c^{+}$PD-$L1^{+}$ cells were in contact with $CD3^{+}$ cells in the gastric mucosa (Figure 12*A* and *B*). There were more $CD11c^{+}$PD-$L1^{+}$ cells in the gastric mucosa of *H pylori*–positive patients than in *H pylori*–negative patients, and the gastric tissue showing mucosal dysplasia had more $CD11c^{+}$PD-$L1^{+}$ cells (Figure 12*C*).

Discussion

In previous in vitro studies, DCs were shown to recognize *H pylori* via pattern recognition receptors such as Toll-like receptors,[40] and *H pylori*–stimulated DCs secrete proinflammatory cytokines such as interleukin (IL)6, IL12, and IL23, and activate co-cultured autologous $CD4^{+}$ T cells to secrete IFN-γ or IL17.[41,42] In contrast to these proinflammatory roles, *H pylori*–stimulated DCs are involved in immune tolerance by inducing Tregs or producing anti-inflammatory cytokines such as IL10 and transforming growth factor β.[14,43] CD11c-DTR mice have been used to understand the in vivo function of gastric DCs in *H pylori* infection.[44,45] However, because DT injection also ablates tissue macrophages in CD11c-DTR mice,[46] DC-specific cell ablation models are required to understand gastric DCs. Meanwhile, 1 study showed that gastric $CD11b^{+}$ DCs engulf *H pylori* in the gastric mucosa.[47] However, the exact immunologic role of gastric DCs in *Helicobacter*-induced gastritis remains largely unknown. In the present study, we showed that the PD-1/PD-L1 pathway plays a critical role in maintaining peripheral T-cell tolerance during *Helicobacter* infection, which appears to be mediated by PD-L1–expressing gastric DCs.

Compared with DCs in other organs, relatively little is known about gastric DCs; thus, we focused on characterizing DCs in the stomach. We defined gastric DCs as a $Ly6G^{-}$Siglec $F^{-}CD64^{-}CD11c^{+}$MHC II^{hi} population and determined that these DCs are composed of $CD103^{+}$, $CD11b^{+}$, and DN subsets. Because macrophages and eosinophils also can express CD11c and MHC II to varying levels and might be contained in the $CD11b^{+}$ subset, we excluded macrophages and eosinophils in advance using CD64, Siglec F, and CD11b markers.[48] The DCs and their subset populations adequately expressed the transcription factors ZBTB46, IRF8, and IRF4, as well as the DC subset surface markers SIRPα, CD24, and XCR1,[25,49–53] and were dependent on the Flt3–Flt3-ligand pathway. Moreover, these populations were ablated by DT injection in *Zbtb46*-DTR BMT mice. From these results, we could confirm that the gastric $Ly6G^{-}$Siglec $F^{-}CD64^{-}CD11c^{+}$MHC II^{hi} population and its subsets are cDCs.

Although expression of the mature DC markers CD103 and CD11b was deficient in the DN subsets, they still can be regarded as bona fide DCs considering their similarity to mature DCs. Recent studies have shown that DN subsets are DC populations in an intermediate maturation stage, and reside in various organs, including the heart, lung, and liver.[26] In the present study, gastric DN subsets showed a 2-peak pattern for the expression of IRF4, IRF8, SIRPα, CD24, and XCR1. These results seem to be consistent with those from another study showing that DN subsets consist of 2 subtypes with the ability to mature into $CD103^{+}$ and $CD11b^{+}$ DCs.[26] Thus, our study suggests that bona fide DN DCs are present in the stomach. Conversely, a few

Figure 7. (***See previous page***). ***Flt3*$^{-/-}$ mice with a decreased number of gastric DCs developed severe gastric inflammation with less *Helicobacter* colonization.** (*A*) Percentage of DCs, DC subsets, and macrophages in live single cells from the stomach of normal *Flt3*$^{-/-}$ and WT mice. Representative flow cytometry plots (*left*). Gastric DCs and all DC subsets, but not macrophages, are deficient in *Flt3*$^{-/-}$ mice (n = 9) compared with WT mice (n = 11). (*B*) Histopathologic analysis of *H felis*–induced gastritis. Representative H&E images of the gastric corpus regions of WT and *Flt3*$^{-/-}$ mice were aligned (*left*). Inflammation score (*right*). Each mouse was scored (n = 13–17 for each group). *Scale bar*: 100 μm. (*C*) Relative PD-L1 mRNA expression levels in gastric corpus tissues from *Flt3*$^{-/-}$ and WT mice after *H felis* infection for 8 weeks. Results are shown as fold change compared with that in the *H felis*–infected WT group (n = 6–7 for each group). (*D*) Localization of *H felis* (*white arrowheads*) in the gastric corpus regions of WT and *Flt3*$^{-/-}$ mice (Warthin–Starry stain) and a manual count of *H felis* in 2 paraffin sections (n = 4–7 for each group). *Scale bar*: 50 μm. (*E*) *H felis* loads were evaluated using quantitative real-time PCR for *H felis* flagellar filament B DNA extracted from the corpus and antrum, respectively (n = 7–10 for each group). (*F*) Level of SP-D in gastric corpus tissues from *Flt3*$^{-/-}$ and WT mice using a magnetic luminex immunoassay (R&D Systems, Minneapolis, MN). Measured protein concentrations (pg/mL) were corrected for total protein content (mg/mL) (n = 7 and 9 for groups with 4 and 8 weeks of *H felis* infection, respectively; n = 5 for noninfection group). Data are presented as means ± SEM. $^{*}P < .05$ and $^{**}P < .01$. Weeks, duration of infection. APC, allophycocyanin.

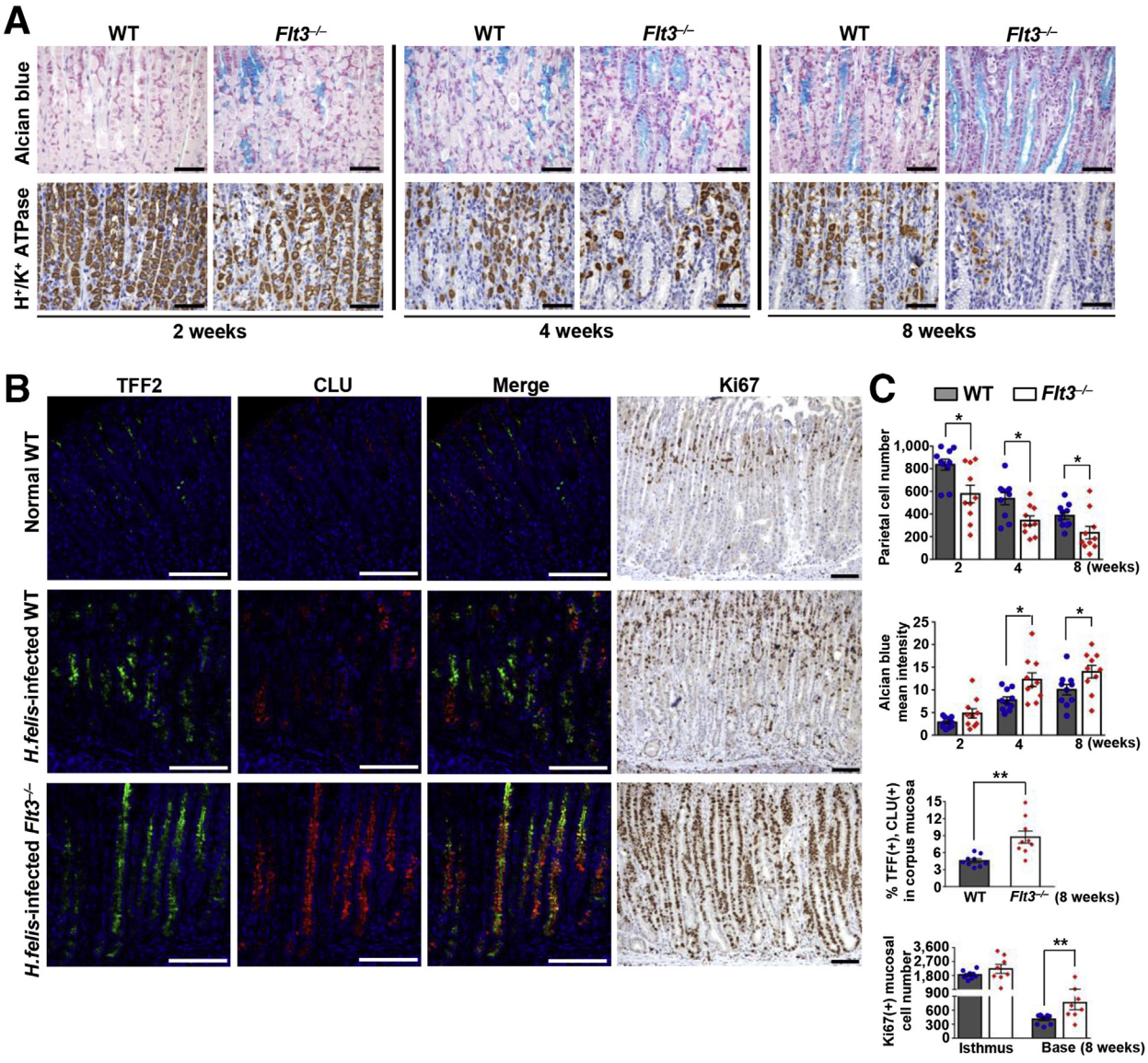

Figure 8. *Flt3*$^{-/-}$ mice have enhanced mucosal metaplasia upon *Helicobacter* infection. (*A–C*) Histopathologic analysis of *H felis*–induced metaplasia of the corpus mucosa. (*A*) Analysis of *H felis*–induced oxyntic atrophy and mucosal metaplasia. Representative serial images of *H felis*–infected WT (*left*) and *H felis*–infected *Flt3*$^{-/-}$ (*right*) mice for Alcian blue staining (*top*) and H^+/K^+-ATPase IHC (*bottom*) were aligned (2, 4, and 8 weeks after *H felis* infection). *Scale bar*: 50 μm. (*B*) Analysis of *H felis*–induced mucosal metaplasia and proliferation. Representative serial images of normal WT (*top*), *H felis* WT (*middle*) and *H felis*–infected *Flt3*$^{-/-}$ (*bottom*) mice after immunostaining for TFF2 (green), CLU (red), and Ki67 (3,3'-diaminobenzidine substrate) were aligned (8 weeks after *H felis* infection). *Scale bar*: 100 μm. (*C*) Quantification of H^+/K^+-ATPase$^+$ cells (parietal cells) (n = 10 for each group), Alcian blue–positive region (n = 10 for each group), TFF2 and CLU double-positive region (WT, n = 9; *Flt3*$^{-/-}$, n = 9), and Ki67-positive cells (WT, n = 9; *Flt3*$^{-/-}$, n = 8) is shown. Data are presented as means ± SEM. **P* < .05 and ***P* < .01. Weeks, duration of infection.

$CD103^+CD11b^+$ cells were found in the gastric DC population. One study considered $CD103^+CD11b^+$ cells as one of the gastric DC subsets.[47] However, in our study, $CD103^+CD11b^+$ cells were not significantly depleted in *Flt3*$^{-/-}$ and DT-treated *Zbtb46*-DTR BMT mice. Although the $CD103^+CD11b^+$ DC subset has been identified in the intestine, further studies are needed to determine whether this population is present in the stomach.

Interestingly, our study highlighted the fact that gastric cDCs are committed to the role of peripheral T-cell tolerance in the stomach during *Helicobacter* infection. One of the immune modulatory mechanisms of DCs is to activate the immune checkpoint pathway of T cells. In our study, during *Helicobacter* infection, gastric DCs were tolerogenic by expressing high levels of PD-L1 and low levels of CD80, CD86, and CD40. It should be noted here that not only the high level of PD-L1 was expressed on DCs, but also the low level of CD80 was expressed on DCs. CD80 of DCs binds cytotoxic T-lymphocyte–associated antigen 4, another co-inhibitory receptor expressed on T cells, or CD28, a co-stimulatory receptor expressed on T cells, but also binds PD-L1 expressed on DCs (*cis*-PD-L1/CD80 interaction) to

disrupt PD-1/PD-L1 binding.[54] Therefore, it is believed that the relative difference in the expression levels of PD-L1 and CD80 on gastric DCs triggered activation of the immune checkpoint pathway.

Furthermore, in *Helicobacter* infection, when cDCs were ablated, a phenotype similar to that noted in the depletion of PD-L1 on leukocytes was observed that included worsened gastritis and pathologic mucosal changes as well as an

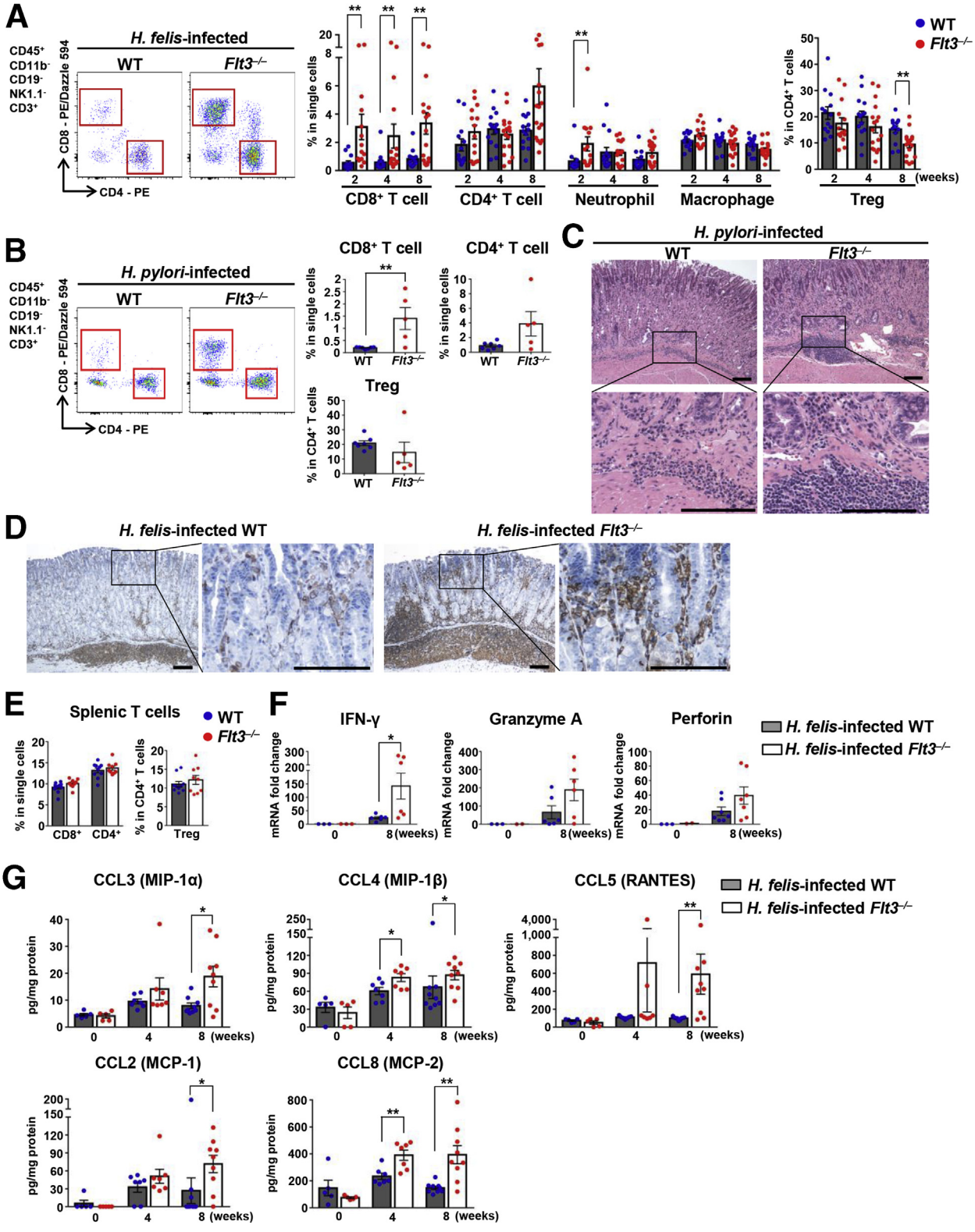

increase in the number of T cells with low bacterial loads. These findings indicate that impairment of cDCs is related to reduced PD-L1 levels in the stomach, which in turn causes a loss of T-cell regulation.

Gastric DCs may inhibit T-cell–mediated immunity through PD-L1 expression by directly regulating the number or activity of T cells or by promoting the differentiation of induced Tregs from conventional CD4$^+$ T cells in the periphery.[55,56] In particular, the in vivo experimental results of our study, such as changes in the Treg population and suboptimal costimulatory state of gastric DCs, support the role of gastric cDCs in promoting Treg development.

Some studies showed that the gastric epithelium expresses PD-L1. These studies used gastric epithelial cell lines[20] or gastric organoid cultures differentiated from human-induced pluripotent stem cells,[23] and thus may not have addressed whether PD-L1 is expressed by leukocytes. In the current study, we observed PD-L1 expression on DCs with flow cytometry of isolated single cells from the whole stomach and IHC on tissue sections of the stomach. With these methods, we identified differences in PD-L1 expression between leukocytes and nonleukocytes, including gastric epithelial cells, and concluded that gastric DCs express considerably higher levels of PD-L1 than gastric epithelial cells.

As mentioned previously, PD-L1$^+$ gastric DCs were located primarily in the submucosa and mucosal laminar propria immediately above the muscularis mucosa with T cells. These DCs are considered a cellular barrier, protecting the gastric mucosa from T-cell infiltration. Without these barrier-functioning DCs, T cells indiscriminately could infiltrate the gastric mucosa and increase the immune response against *Helicobacter* infection by promoting the mobilization of other immune cells such as neutrophils,[57] thereby decreasing bacterial loads but also inadvertently causing damage to the mucosa. During *Helicobacter* infection, mucosal damage is accompanied by the loss of parietal cells and mature chief cells (atrophy), SPEM, and further intestinal metaplasia as the lesion becomes more severe.[58] Mucosal metaplasia has been regarded as a precancerous lesion because it is closely related to the incidence of gastric cancer in human beings.[59] Interestingly, when DCs are absent, worsened oxyntic atrophy and mucosal metaplasia are accompanied by an increase in T-cell accumulation in the gastric mucosa. Gastric DCs may be involved in defense mechanisms against carcinogenesis by slowing the progression of gastritis into gastric cancer. However, considering that a recent study reported an association between immune stromal PD-L1 expression and poor prognosis in patients with gastric adenocarcinoma,[10] and the fact that our results showed co-localization of PD-L1$^+$ gastric DCs with T cells in some patients with mucosal dysplasia, suppression of T cells by gastric DCs via PD-L1 could have either a deleterious or a beneficial effect on the host, depending on the pathologic progression of the gastric lesions.

Along with other immune checkpoint inhibitors, PD-1 and PD-L1 inhibitors have been highlighted as a novel anticancer therapy. Some of them have received Food and Drug Administration approval and have proven effective, thereby increasing expectations. However, these inhibitors are reported to have inflammatory side effects called immune-related adverse events (IRAEs), and the stomach is one of the most IRAE-prone organs.[60–62] Thus, the possibility of IRAE occurrence in the stomach should be an important consideration when treating cancer patients with checkpoint inhibitors. The inflammatory events shown in the current study might provide the basis to elucidate mechanisms underlying IRAE occurrence in the stomach.

In conclusion, we finely characterized gastric DCs in gastritis caused by *Helicobacter* infection. Moreover, the immune modulatory function of gastric cDCs possibly by the PD-1/PD-L1 pathway importantly protects the gastric mucosa against lymphocytic inflammation and precancerous mucosal changes, but allows persistent bacterial colonization. Our findings show that gastric cDCs are key immune cells that fine-tune inflammatory processes and bacterial colonization in *Helicobacter*-infected gastric mucosa.

Materials and Methods

Human Gastric Tissue Samples

Formalin-fixed paraffin-embedded tissue samples (20 *H pylori*–negative patients, 31 *H pylori*–positive patients, and 46 patients with mucosal dysplasia) from surgically resected human gastric tissue were retrieved from the archives of the Department of Pathology, Seoul National University Bundang Hospital (Seongnam, Korea). The collected tissue samples were the samples remaining after proper histologic diagnosis and relevant molecular study. Representative tissue areas were reviewed and selected for the construction of a tissue microarray. The study was approved by the

Figure 9. (***See previous page***). ***Flt3*$^{-/-}$ mice show more prominent CD8$^+$ T-cell accumulation upon *Helicobacter* infection.** (*A*) Percentage of CD8$^+$ T cells, CD4$^+$ T cells, neutrophils, and macrophages in live single cells and of Tregs in live CD4$^+$ T cells from the stomach of *Flt3*$^{-/-}$ and WT mice with *H felis* infection (n = 13–17 for each *H felis* infection group, n = 9–11 for the noninfection group). Representative flow cytometry plots of T cells (*left*). (*B*) As in panel *A*, but with *H pylori* infection (WT, n = 7; *Flt3*$^{-/-}$, n = 5). Note that the number of CD8$^+$ T cells is higher in *Flt3*$^{-/-}$ mice. (*C*) Representative H&E images of the gastric corpus regions of *H pylori*–infected WT (*left*) and *H pylori*–infected *Flt3*$^{-/-}$ (*right*) mice were aligned. *Scale bar*: 200 μm. (*D*) More severe mucosal infiltration of T cells in the stomach of *H felis*–infected *Flt3*$^{-/-}$ mice. Representative images of CD3 IHC (3,3'-diaminobenzidine substrate). *Scale bar*: 200 μm. (*E*) The T-cell fraction in the spleens of WT and *Flt3*$^{-/-}$ mice 8 weeks after *H felis* infection. Note that DC depletion did not affect CD8$^+$ T cells, CD4$^+$ T cells, or the Treg population in the spleen (WT, n = 10; *Flt3*$^{-/-}$, n = 9). (*F*) Relative IFN-γ, Granzyme A, and Perforin mRNA expression levels in gastric corpus tissues from *Flt3*$^{-/-}$ and WT mice after *H felis* infection for 8 weeks. Results are shown as fold change compared with the noninfected WT group (n = 6–7 for the *H felis* infection group, n = 2–3 for the noninfection group). (*G*) Chemokine levels in gastric corpus tissues from *Flt3*$^{-/-}$ and WT mice using a magnetic Luminex immunoassay. Measured protein concentrations (pg/mL) were corrected for total protein content (mg/mL) (n = 7 and 9 for groups with 4 and 8 weeks of *H felis* infection, respectively; n = 5 for noninfection group). Data are presented as means ± SEM. **P* < .05 and ***P* < .01. Weeks, duration of infection.

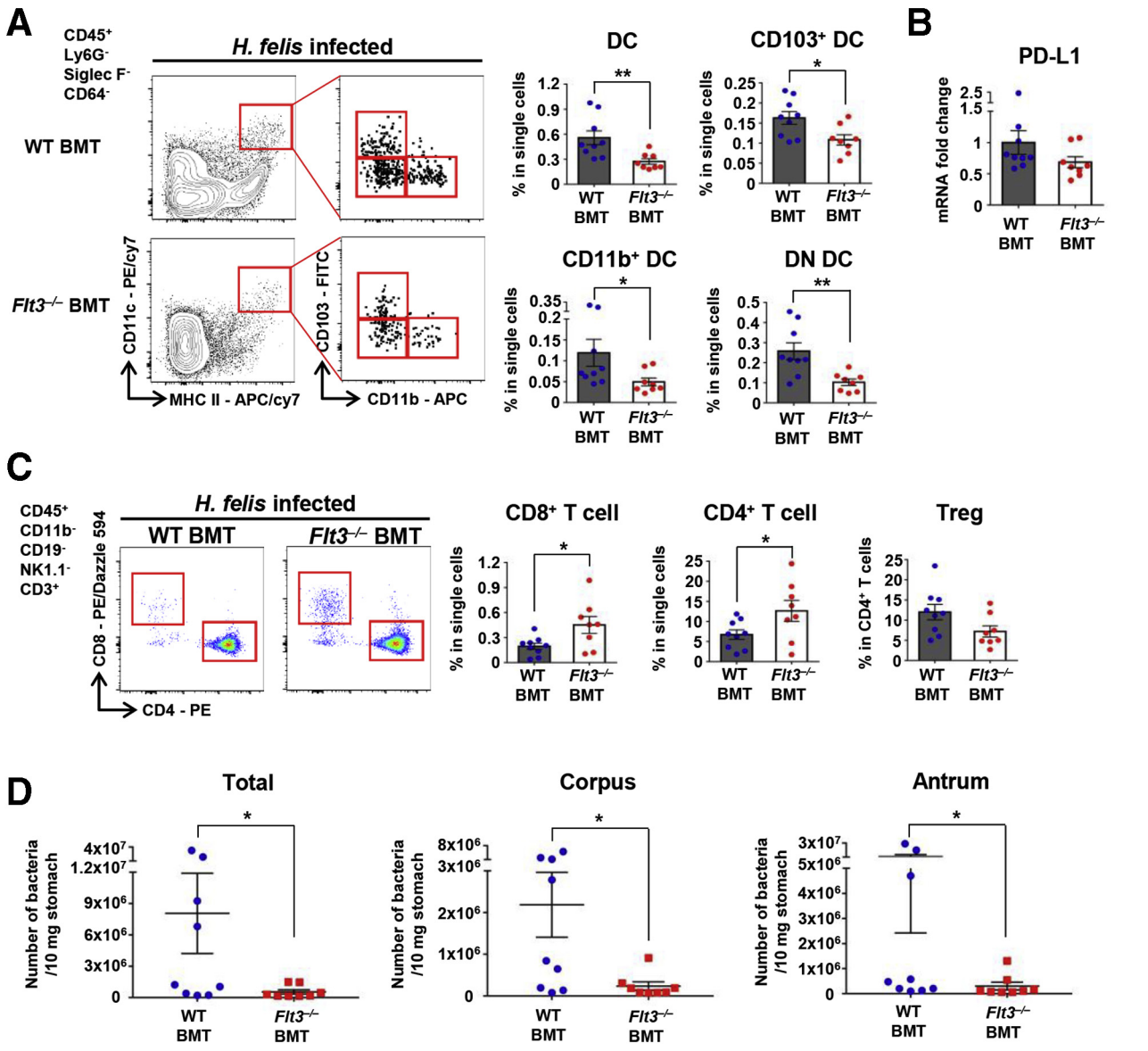

Figure 10. *Flt3*$^{-/-}$ BMT mice with a decreased number of gastric DCs developed prominent T-cell responses with less *Helicobacter* colonization after *H felis* infection for 8 weeks. (*A*) The percentage of DCs and DC subsets in live single cells from the stomach of *Flt3*$^{-/-}$ BMT (n = 8) and WT BMT (n = 9) mice. Representative flow cytometry plots (*left panel*). (*B*) Relative PD-L1 mRNA expression levels in gastric corpus tissues from *Flt3*$^{-/-}$ BMT (n = 8) and WT BMT (n = 9) mice 8 weeks after *H felis* infection. Results are shown as fold change compared with that in the *H felis*–infected WT BMT group. (*C*) Percentage of CD8^{+} T cells and CD4^{+} T cells in live single cells and of Tregs in live CD4^{+} T cells from the stomach of *Flt3*$^{-/-}$ BMT (n = 8) and WT BMT (n = 9) mice. Representative flow cytometry plots (*left panel*). (*D*) *H felis* loads were evaluated using quantitative real-time PCR for *H felis* flagellar filament B DNA extracted from the corpus and antrum, respectively (WT BMT, n = 9; *Flt3*$^{-/-}$ BMT, n = 8). Data are presented as means ± SEM. *$P < .05$ and **$P < .01$. APC, allophycocyanin; PE, phycoerythrin.

Institutional Review Board of the Seoul National University Bundang Hospital (Institutional Review Board number: B-1606/349-308) and the Seoul National University Hospital (Institutional Review Board number: 1706-105-860) and performed in accordance with the principles of the Declaration of Helsinki. Informed consent was waived.

Mice

Flt3$^{-/-}$ mice[63] were a generous gift from Professor Ihor R. Lemischka (Developmental and Stem Cell Biology, Mount Sinai School of Medicine, New York, NY). *Flt3*$^{-/-}$, B6(Cg)-*Zbtb46*$^{tm1(HBEGF)Mnz}$/J (*Zbtb46*-DTR, stock 019506; The Jackson Laboratory, Bar Harbor, ME), C57BL/6-Tg(CLEC4C-HBEGF)956Cln/J (*BDCA2*-DTR, stock 014176; The Jackson Laboratory), and B6.Cg-Tg(Itgax-Venus)1Mnz/J (CD11c-Enhanced Yellow Fluorescent Protein (EYFP), stock 008829; The Jackson Laboratory) mice on a C57BL/6J background were housed individually in the animal facility of Seoul National University or Hanyang University and provided a normal mouse diet and water ad libitum. Male C57BL/6J mice were purchased from Japan SLC, Inc (Hamamatsu, Shizuoka, Japan) through the Central Lab Animal, Inc (Seoul, Korea). All

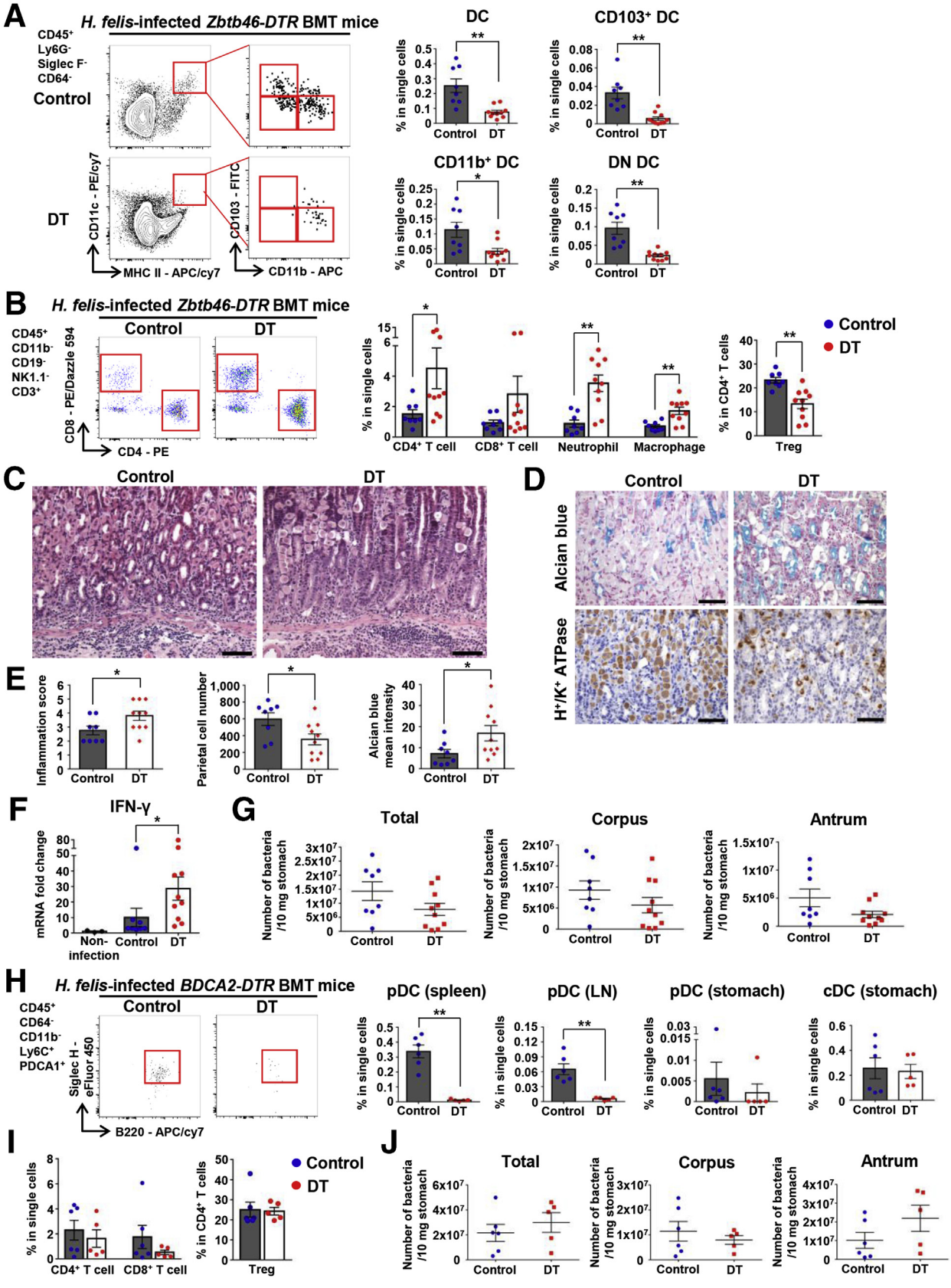
A
H. felis-infected Zbtb46-DTR BMT mice
CD45+ Ly6G- Siglec F- CD64-
Control
DT
CD11c - PE/cy7
MHC II - APC/cy7
CD103 - FITC
CD11b - APC
DC
CD103+ DC
CD11b+ DC
DN DC
% in single cells
Control
DT
B
H. felis-infected Zbtb46-DTR BMT mice
CD45+ CD11b- CD19- NK1.1- CD3+
CD8 - PE/Dazzle 594
CD4 - PE
CD4+ T cell
CD8+ T cell
Neutrophil
Macrophage
% in CD4+ T cells
Treg
C
D
Alcian blue
H+/K+ ATPase
E
Inflammation score
Parietal cell number
Alcian blue mean intensity
F
IFN-γ
mRNA fold change
Non-infection
G
Total
Corpus
Antrum
Number of bacteria /10 mg stomach
H
H. felis-infected BDCA2-DTR BMT mice
CD45+ CD64- CD11b- Ly6C+ PDCA1+
Siglec H - eFluor 450
B220 - APC/cy7
pDC (spleen)
pDC (LN)
pDC (stomach)
cDC (stomach)
I
J

mice experiments were approved by the Animal Care and Use Committees of Seoul National University or Hanyang University (certification numbers: SNU-140320-2-9 and HY-IACUC-18-0048).

BM Transplantation

BM cells from *Flt3*$^{-/-}$, *Zbtb46*-DTR, *BDCA2*-DTR, or *Pdl1*$^{-/-}$ mice[64] (housed in the animal facility of Yonsei University) were injected intravenously into lethally irradiated (500 rad twice, 3-hour interval) WT C57BL/6J mice. BMT mice were fed water containing 7.6% Baytril (Bayer Korea, Seoul, Korea) for 2 weeks and monitored for approximately 6 weeks, until the transplanted BM was effectively reconstructed.

DT Injection

cDCs and pDCs were depleted via intraperitoneal administration of DT (322326; Calbiochem, San Diego, CA) to *Zbtb46*-DTR BMT mice and *BDCA2*-DTR BMT mice, respectively. A total of 500 ng DT was injected 2 days before *H felis* infection. During the infection period, *Zbtb46*-DTR BMT mice were treated with 100 ng DT every 2 days, and *BDCA2*-DTR BMT mice were treated with 200 ng DT every 3 days. The control group was treated with phosphate-buffered saline instead of DT, following the same schedule.

In Vivo PD-L1 Blockade

Anti-mouse PD-L1 (B7-H1) antibody (BE0101; Bio X Cell, West Lebanon, NH) was administered intraperitoneally to *H felis*–infected mice to block the PD-1/PD-L1 pathway during *H felis* infection. A total of 300 μg PD-L1 antibody diluted in *InVivo*Pure pH 6.5 Dilution Buffer (IP0065; Bio X Cell) was administered 6 times, once every 3 days, before necropsy. A rat IgG2b isotype antibody (BE0090; Bio X Cell) diluted in *InVivo*Pure pH 7.0 Dilution Buffer (IP0070; Bio X Cell) was used as a control.

Helicobacter *Culture and Infection*

H felis (ATCC 49179) was cultured in sterile-filtered brucella broth (211088; Becton Dickinson, Sparks, MD) containing 10% fetal bovine serum (FBS). Mouse-adapted *H pylori* Sydney strain 1[65] was cultured on the Brain Heart Infusion Agar plates (241830; Becton Dickinson) containing 10% sheep blood and *H pylori* Selective Supplement (SR0147E; Thermo Fisher Scientific, Rockford, IL). The brucella broth and brain heart infusion agar plates were maintained under microaerobic conditions produced using a GasPak EZ Campy Container System (260680; Becton Dickinson) at 37°C. The brucella broth was maintained at 150 rpm shaking. After 24-hour fasting, 8-week-old mice were orally administered 0.2 mL suspension containing 2×10^8 *H felis* or 1×10^9 colony-forming unit/mL *H pylori* 4 times every other day.

Necropsy and Tissue Preparation

At 2, 4, and 8 weeks after *H felis* infection, each group of mice was killed together with the noninfected control group, and the stomach, gastric lymph node, and spleen were removed. The stomach was incised along the greater curvature and spread onto filter paper. After cutting the lesser curvature, half of the stomach was used for flow cytometry and *H felis* quantification. The lesser curvature portion of the other half was fixed in 10% neutral buffered formalin for histopathologic examination, and the remaining tissue was stored at -70°C for subsequent analysis. At 18 months after *H pylori* infection, the *H pylori*–infected groups were treated as described previously.

Histopathologic Examinations and Quantitation

Gastric tissues fixed in 10% neutral buffered formalin were cut into 2 strips. After standard tissue processing, gastric tissues were embedded in paraffin wax. Paraffin sections were stained with H&E or an Alcian blue (pH 2.5) stain kit (H-3501; Vector Laboratories, Burlingame, CA). IHC for H^+/K^+-ATPase, TFF2, CLU, and Ki67 was performed to assess histopathologic changes. The degree of gastritis and pathologic mucosal changes were assessed based on methods described previously.[19,66,67] Briefly, we graded the lesion with a scale of 0–6. The definition of inflammation

Figure 11. (***See previous page***). **Depletion of cDCs enhances *Helicobacter*-induced gastric inflammation.** (*A*) Percentage of DCs and DC subsets in live single cells from the stomach of DT-injected *Zbtb46*-DTR BMT mice (cDC-ablated mice; n = 10) and PBS-injected *Zbtb46*-DTR BMT mice (control mice; n = 8) 4 weeks after *H felis* infection. Representative flow cytometry plots (*left*). Note that gastric DCs and DC subsets are *Zbtb46*-dependent cDCs. (*B*) Percentage of $CD8^+$ T cells, $CD4^+$ T cells, neutrophils, and macrophages in live single cells and of Tregs in live $CD4^+$ T cells from the stomach of cDC-ablated (n = 10) and control (n = 8) mice. Representative flow cytometry plots of T cells (*left*). (*C*) Histopathologic analysis of *H felis*–induced gastritis. Representative H&E images of the gastric corpus regions of control (*left*) and cDC-ablated (*right*) mice. *Scale bar*: 100 μm. (*D*) Histopathologic analysis of *H felis*–induced oxyntic atrophy and mucosal metaplasia. Representative serial images of the gastric corpus regions of control (*left*) and cDC-ablated (*right*) mice after Alcian blue staining (*top*) and H^+/K^+-ATPase IHC (*bottom*). *Scale bar*: 50 μm. (*E*) Inflammation score (*left*) and quantification of H^+/K^+-ATPase$^+$ cells (parietal cells) (*middle*), and Alcian blue–positive region (*right*) (control mice, n = 8; cDC-ablated mice, n = 10). (*F*) Relative gastric mRNA expression levels of IFN-γ. Results are shown as fold change compared with the noninfection group (noninfection group, n = 3; control group, n = 8; cDC-ablated group, n = 10). (*G*) bacterial loads were evaluated using quantitative real-time PCR for *H felis* flagellar filament B DNA extracted from the corpus and antrum, respectively (control mice, n = 8; cDC-ablated mice, n = 10). (*H*) Percentage of pDCs (spleen, gastric lymph node [LN], and stomach) and cDCs (stomach) in live single cells of DT-injected *BDCA2*-DTR BMT mice (pDC-ablated mice; n = 5) and PBS-injected *BDCA2*-DTR BMT mice (control; n = 6). Representative pDCs flow cytometry plot of 4 pooled stomachs per group (*left*). (*I*) Percentage of $CD8^+$ T cells and $CD4^+$ T cells in live single cells and of Tregs in live $CD4^+$ T cells from the stomach of pDC-ablated mice (n = 5) and control mice (n = 6). (*J*) Bacterial loads were evaluated using quantitative real-time PCR for *H felis* flagellar filament B DNA extracted from the corpus and antrum, respectively (control mice, n = 6; pDC-ablated mice, n = 5). Data are presented as means ± SEM. **P* < .05 and ***P* < .01. Weeks, duration of infection. PE, phycoerythrin.

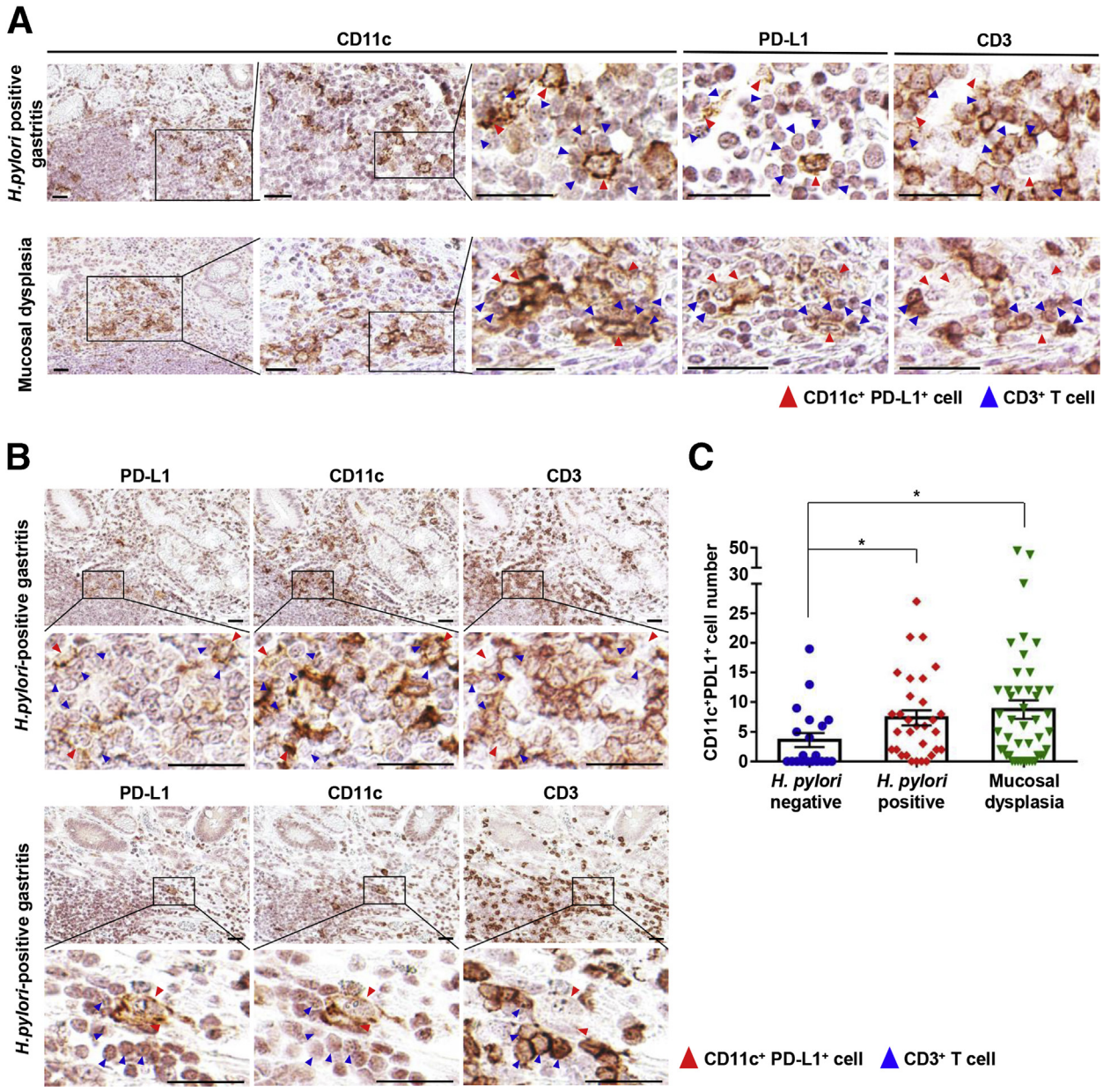

Figure 12. PD-L1–expressing DCs co-localize with T cells in human *Helicobacter*-positive gastritis. (*A*) Multiplexed IHC-stained representative images of the stomach of *H pylori*–positive patients (*top*) and patients with mucosal dysplasia (*bottom*). Multiplexed IHC was performed sequentially on each single section in the order of PD-L1, CD11c, and CD3. After each immunostained section was scanned, the section was placed in antibody stripping buffer to erase the staining and subjected to another immunostaining. Note that PD-L1$^+$CD11c$^+$ cells (*red arrowheads*) co-localize with CD3$^+$ cells (*blue arrowheads*). *Scale bar*: 30 μm. (*B*) Multiplexed IHC stained representative images of the stomach of other *H pylori*–positive patients. Note that the positions of PD-L1$^+$ and CD11c$^+$ cells are similar (low-power fields) and PD-L1$^+$CD11c$^+$ cells (*red arrowheads*) co-localize with CD3$^+$ cells (*blue arrowheads*) (high-power fields). *Scale bar*: 30 μm. (*C*) Quantification of PD-L1$^+$CD11c$^+$ cells in a section of a biopsy sample (*H pylori*–negative sample, n = 21; *H pylori*–positive sample, n = 31; mucosal dysplasia sample, n = 46). Data are presented as means ± SEM. *$P < .05$.

scores are as follows: 0, none; 1, some infiltrates; 2, mild (few aggregates in submucosa and mucosa); 3, moderate (several aggregates in submucosa and mucosa); 4, marked (many aggregates in submucosa and mucosa); 5, nearly the entire mucosa contains a dense infiltrate; and 6, entire mucosa contains a dense infiltrate. Scores for pathologic mucosal changes were as follows: 0, none; 1, foci in which a few gastric glands are lost or replaced; 2, small areas in which gastric glands are lost or replaced; 3, less than 25% of gastric glands are lost or replaced; 4, 25%–50% of gastric glands are lost or replaced; 5, more than 50% of gastric glands are lost or replaced; and 6, only a few small areas of gastric glands remaining. Quantitation of Alcian blue–positive mucin and H^+/K^+-ATPase–, Ki67-, TFF2-, and CLU-positive cells was performed at the representative same region within the corpus mucosa for each sample. The

Table 1. List of Antibodies for Flow Cytometry

Antibody	Clone	Catalog number	Source
CD103	2E7	11-1031-81	eBioscience (San Diego, CA)
Foxp3	FJK-16s	17-5773-82	eBioscience
IRF8	V3GYWCH	17-9852	eBioscience
IRF4	3E4	48-9858-80	eBioscience
CD40	1C10	17-0401-81	eBioscience
Siglec-H	eBio440c	48-0333-80	eBioscience
Rat IgG1κ isotype	eBRG1	48-4301-80	eBioscience
CD4	GK1.5	553730	BD Bioscience
Zbtb46	U4-1374	565832	BD Bioscience
PD-L2	TY25	564245	BD Bioscience
Siglec-F	E50-2440	562681	BD Bioscience
CD24	M1/69	563060	BD Bioscience
CD11b	M1/70	101206, 101216, 101212, 101226	BioLegend
CD64	X54-5/7.1	139304, 139320	BioLegend
MHC II	M5/114.15.2	107621, 107628	BioLegend
Ly6C	HK1.4	128006	BioLegend
CD45	30-F11	103130	BioLegend
CD11c	N418	117318	BioLegend
NK1.1	PK136	108714	BioLegend
CD8α	53-6.7	100762	BioLegend
F4/80	BM8	123146, 123149	BioLegend
PDCA-1	927	127015	BioLegend
CD86	GL-1	105012	BioLegend
CD19	6D5	115527	BioLegend
B220	RA3-6B2	103223	BioLegend
PD-L1	10F.9G2	124308, 124315	BioLegend
CD3	17A2	100228	BioLegend
CD80	16-10A1	104725	BioLegend
Ly6G	1A8	127607, 127639, 127641	BioLegend
XCR1	ZET	148220	BioLegend
Siglec-F	S17007L	155505	BioLegend
SIRPα	P84	144015	BioLegend
Armenian hamster IgG Isotype	HTK888	400905, 400921	BioLegend
Rat IgG2α, κ Isotype	RTK2758	400505, 400507, 400511, 400526, 400540, 400542, 400549, 400557	BioLegend

number of H^+/K^+-ATPase–positive cells was counted manually. The amount of Alcian blue–positive mucin was measured using mean intensity with ImageJ software (National Institutes of Health, Bethesda, MD). The number of Ki67-positive cells was counted using ImageJ software. TFF2 and CLU expression was quantified by measuring the area of each positive signal region using CaseViewer software (3d Histech, Budapest, Hungary). Slides were imaged digitally using a Pannoramic scanner (3d Histech).

Single-Cell Preparations and Flow Cytometric Analysis

Gastric tissues were incubated in Hank's balanced salt solution containing 2 mmol/L EDTA (CMS005; Cosmo Genetech, Seoul, Korea), 2% FBS, and 1 mmol/L DL-dithiothreitol (D0632-1G; Sigma-Aldrich, St. Louis, MO) for 15 minutes at 37°C with shaking. Next, the gastric tissue was finely trimmed and ground using gentleMACS Dissociator (130-093-235; Miltenyi Biotec, Bergisch Gladbach, Germany) and incubated in Hank's balanced salt solution containing 100 U/mL collagenase D (11088866001; Roche, Mannheim, Germany), 10% FBS, 10 mmol/L HEPES (SH30237.01; GE Healthcare Life Sciences, Logan, UT), and 90 U/mL DNase 1 (4716728001; Roche) for 30 minutes at 37°C with shaking. After incubation, the gastric tissue was ground once more using the gentleMACS Dissociator, filtered through a 70-μm cell strainer, and centrifuged to collect the single cells. The final single cells were prepared by combining the cells collected from the suspension and from the gastric tissue. Gastric lymph node and spleen were incubated with 400 U/mL collagenase D at 37°C for 20

Table 2. List of Primary Antibodies for Immunohistochemistry and Immunofluorescence

Antibody	Clone	Catalog no.	Source	Dilution
CD3	Polyclonal	A0452	Dako	1:200 (paraffin)
CD3	17A2	100201	BioLegend	1:50 (frozen)
CD45	30-F11	103101	BioLegend	1:100 (frozen)
CD11c	D1V9Y	97585	Cell Signaling Technology	1:400 (paraffin)
CD11c	HL3	550283	BD Biosciences	1:100 (frozen)
PD-1	D7D5W	84651	Cell Signaling Technology	1:50 (frozen)
PD-L1	Polyclonal	PA5-20343	Invitrogen	1:100 (frozen)
H^+/K^+-ATPase	2B6	D032-3H	MBL (Tokyo, Japan)	1:4000 (paraffin)
TFF2	Polyclonal	13681-1-AP	Proteintech (Rosemont, IL)	1:400 (paraffin)
Clusterin	Polyclonal	AF2747	R&D Systems	1:400 (paraffin)
Ki67	Polyclonal	ab15580	Abcam	1:200 (paraffin)

minutes to obtain dissociated single cells. The prepared single cells were stained primarily with Zombie Aqua (423102; BioLegend, San Diego, CA) to discriminate dead cells, according to the manufacturer's protocol. Zombie Aqua–stained cells then were processed for Fragment crystallizable (Fc) receptor block by using a TruStain FcX antibody (anti-CD16/32, clone 93, 101320; BioLegend), to avoid nonspecific binding. After blocking, cells were incubated with a mixture of fluorochrome-labeled antibodies at 4°C for 30 minutes. To stain for transcription factors (Forkhead box P3 [FOXP3], IRF4, IRF8, and ZBTB46), cells were fixed and permeabilized with a FOXP3/Transcription Factor Staining Buffer Set (00-5523-00; Thermo Fisher Scientific), according to the manufacturer's protocol, and stained with an antibody against each transcription factor. Antibodies are listed in Table 1. After washing briefly with RPMI 1640 medium containing 10% FBS, cells were analyzed using BD LSRFortessa (BD Biosciences, San Jose, CA) and FlowJo software (version 9.9 and 10.4; developed by FlowJo, LLC, Ashland, OR).

Immunohistochemistry and Immunofluorescence

Paraffin sections were dewaxed and hydrated, and then antigen retrieval was performed using pH 6.0 citrate buffer (C9999; Sigma-Aldrich). Next, when visualizing the signal with 3,3'-diaminobenzidine substrate, sections were incubated with 0.3% hydrogen peroxide solution for 30 minutes to block endogenous peroxidase activity. An ImmPRESS Peroxidase Polymer kit (Vector Laboratories) was used according to the manufacturer's protocol. Briefly, paraffin sections were blocked with 2.5% normal horse or goat serum for 1 hour and then incubated with the primary antibodies at 4°C overnight or at 20°C for 2 hours. The primary antibodies are listed in Table 2. For chromogenic detection, sections were incubated with an appropriate horseradish-peroxidase–conjugated secondary antibody (Vector Laboratories) for 1 hour followed by ImmPACT 3,3'-diaminobenzidine substrate (SK-4105; Vector Laboratories) and counterstained with hematoxylin. For fluorescence detection, Alexa488-conjugated donkey anti-rabbit IgG (Jackson ImmunoResearch, West Grove, PA) and Cy3-conjugated donkey anti-goat IgG (Jackson ImmunoResearch) were used at a 1:400 dilution. Sections were counterstained with 4′,6-diamidino-2-phenylindole (62248; Thermo Fisher Scientific) and mounted using mounting medium (Vector Laboratories). For anti-H^+/K^+-ATPase IHC, a Mouse on Mouse ImmPRESS Peroxidase Polymer Kit (MP-2400; Vector Laboratories) was used to block endogenous mouse immunoglobulin.

Frozen sections were blocked with 2.5% normal goat serum (Vector Laboratories) for 1 hour and incubated with primary antibodies (Table 2) overnight at 4°C. For fluorescence detection, Alexa594-conjugated goat anti-rat IgG (Jackson ImmunoResearch), Alexa488-conjugated goat anti-Armenian hamster IgG (Jackson ImmunoResearch), Alexa488-conjugated donkey anti-rabbit IgG (Jackson ImmunoResearch), and Alexa488- or Alexa594-conjugated goat anti-rabbit IgG (Invitrogen, Carlsbad, CA) were used at a 1:400 dilution. Sections were counterstained with 4′,6-diamidino-2-phenylindole and mounted using mounting medium (Vector Laboratories). Images were obtained using a confocal fluorescence microscope (Eclipse TE2000; Nikon, Tokyo, Japan; and LSM 800; Zeiss, Oberkochen, Germany).

H felis *Quantification*

Total DNA was extracted from gastric tissues (corpus and antrum) using a QIAamp DNA mini kit (51304; Qiagen, Hilden, Germany) and used to identify *H felis* DNA. Quantitative real-time polymerase chain reaction (PCR) was performed using specific primers for *H felis* flagellar filament B, Rotor-Gene SYBR Green PCR kit (204074; Qiagen), and Rotor-Gene Q (Qiagen). Amplified target DNA was analyzed using Rotor-Gene Q series software. The *H felis* flagellar filament B primers: forward: 5′-TTCGATTGGTCCTACAGGCTCAGA-3′ and reverse: 5′-TTCTTGTTGATGACATTGACCAACGCA-3′ were used.[68] A Warthin–Starry staining kit (ab150688; Abcam, Cambridge, UK) was used to identify the location of *H felis* and to assess the extent of colonization in the stomach. Colonized *H felis* were counted manually on 2 sections from each sample.

Table 3. List of Primers for Quantitative Real-Time Reverse-Transcription PCR

Primer name	Sequence
Mouse GAPDH forward	5′-TGCACCACCAACTGCTTAG-3′
Mouse GAPDH reverse	5′-GGATGCAGGGATGATGTTC-3′
Mouse IFN-γ forward	5′-AGCGGCTGACTGAACTCAGATTGTAG-3′
Mouse IFN-γ reverse	5′-GTCACAGTTTTCAGCTGTATAGGG-3′
Mouse PD-L1 forward	5′-TGGACAAACAGTGACCACCAA-3′
Mouse PD-L1 reverse	5′-CCCCTCTGTCCGGGAAGT-3′
Mouse IL10 forward	5′-GCTCCAAGACCAAGGTGTCT-3′
Mouse IL10 reverse	5′-CTAGGTCCTGGAGTCCAGCA-3′
Mouse TGF-β forward	5′-CTTCAATACGTCAGACATTCGGG-3′
Mouse TGF-β reverse	5′-GTAACGCCAGGAATTGTTGCTA-3′

GAPDH, glyceraldehyde-3-phosphate dehydrogenase; TGF-β, transforming growth factor β.

Quantitative Real-Time Reverse-Transcription PCR

Total RNA from gastric corpus tissues was extracted using a Hybrid-R RNA purification kit (305-101; GeneAll, Seoul, Korea). Complementary DNA was synthesized from 0.1 μg RNA using a QuantiTect Reverse Transcription kit (205313; Qiagen). Quantitative real-time PCR was performed using specific primers, Rotor-Gene SYBR Green PCR kit (204074; Qiagen), and Rotor-Gene Q (Qiagen). The amplified target complementary DNA was analyzed using Rotor-Gene Q series software against the housekeeping gene glyceraldehyde-3-phosphate dehydrogenase. Specific primer sequences are listed in Table 3. Primers for mouse Granzyme A (QT01551690) and perforin (QT00282002) were purchased from Qiagen.

Magnetic Luminex Immunoassay

For protein extraction, gastric corpus tissues of *H felis*–infected and noninfected WT and *Flt3*$^{-/-}$ mice were lysed using Cell Lysis Buffer 2 (895347; R&D Systems, Minneapolis, MN). Chemokine and cytokine protein concentrations were measured using the Mouse Premixed Multi-Analyte kit (LXSAMSM; R&D Systems) according to the manufacturer's protocol.

Multiplexed Immunohistochemistry

Multiplexed IHC was performed sequentially on each single paraffin section in the order of PD-L1, CD11c, and CD3 using Autostainer Link48 (Dako, Glostrup, Denmark) as previously described.[69] Primary antibodies were as follows: rabbit anti–PD-L1 (1:30, 13684; Cell Signaling Technology, Danvers, MA), rabbit anti-CD11c (1:100, ab52632; Abcam), and rabbit anti-CD3 (1:300, A0452; Dako). After the immunostained sections were scanned using the Aperio AT2 (Leica Biosystems, Newcastle, UK), the slides were incubated in premixed stripping buffer (20% sodium dodecyl sulfate, 0.5 mol/L Tris-HCl pH 6.8, β-mercaptoethanol, and distilled water) for antibody stripping. For more effective stripping, slides were microwaved on low power. Sections then were incubated with the next primary antibody. For quantitation of PD-L1–expressing gastric DCs, $CD11c^{+}PD\text{-}L1^{+}$ cells were counted manually using QuPath software (available: https://qupath.github.io) on digitally scanned sections.

Statistical Analysis

All data are shown as means ± SE. Statistical analysis was performed using GraphPad Prism 7.00 (GraphPad Software, San Diego, CA). Two groups were compared using the Mann–Whitney *U* test or an unpaired *t* test with 2-tailed distributions after a Shapiro–Wilk normality test. When 3 or more groups were included, results were analyzed using the Kruskal–Wallis test or ordinary 1-way analysis of variance followed by the Mann–Whitney *U* test or an unpaired *t* test with 2-tailed distributions. A *P* value less than .05 was considered significant. All authors had access to the study data and reviewed and approved the final manuscript.

References

1. Arasanz H, Gato-Cañas M, Zuazo M, Ibañez-Vea M, Breckpot K, Kochan G, Escors D. PD1 signal transduction pathways in T cells. Oncotarget 2017; 8:51936–51945.
2. Fife BT, Pauken KE, Eagar TN, Obu T, Wu J, Tang Q, Azuma M, Krummel MF, Bluestone JA. Interactions between PD-1 and PD-L1 promote tolerance by blocking the TCR-induced stop signal. Nat Immunol 2009; 10:1185–1192.
3. Wherry EJ. T cell exhaustion. Nat Immunol 2011; 12:492–499.
4. Chikuma S, Terawaki S, Hayashi T, Nabeshima R, Yoshida T, Shibayama S, Okazaki T, Honjo T. PD-1-mediated suppression of IL-2 production induces CD8+ T cell anergy in vivo. J Immunol 2009;182:6682–6689.
5. Dong H, Strome SE, Salomao DR, Tamura H, Hirano F, Flies DB, Roche PC, Lu J, Zhu G, Tamada K, Lennon VA, Celis E, Chen L. Tumor-associated B7-H1 promotes T-cell apoptosis: a potential mechanism of immune evasion. Nat Med 2002;8:793–800.
6. Patsoukis N, Sari D, Boussiotis VA. PD-1 inhibits T cell proliferation by upregulating p27 and p15 and suppressing Cdc25A. Cell Cycle 2012;11:4305–4309.
7. Jubel JM, Barbati ZR, Burger C, Wirtz DC, Schildberg FA. The role of PD-1 in acute and chronic Infection. Front Immunol 2020;11:487.
8. Sharpe AH, Wherry EJ, Ahmed R, Freeman GJ. The function of programmed cell death 1 and its ligands in regulating autoimmunity and infection. Nat Immunol 2007;8:239–245.

9. Kronsteiner B, Bassaganya-Riera J, Philipson N, Hontecillas R. Novel insights on the role of CD8+ T cells and cytotoxic responses during Helicobacter pylori infection. Gut Microbes 2014;5:357–362.
10. Thompson ED, Zahurak M, Murphy A, Cornish T, Cuka N, Abdelfatah E, Yang S, Duncan M, Ahuja N, Taube JM, Anders RA, Kelly RJ. Patterns of PD-L1 expression and CD8 T cell infiltration in gastric adenocarcinomas and associated immune stroma. Gut 2017; 66:794–801.
11. Kusters JG, van Vliet AH, Kuipers EJ. Pathogenesis of Helicobacter pylori infection. Clin Microbiol Rev 2006; 9:449–490.
12. Bimczok D, Clements RH, Waites KB, Novak L, Eckhoff DE, Mannon PJ, Smith PD, Smythies LE. Human primary gastric dendritic cells induce a Th1 response to H. pylori. Mucosal Immunol 2010;3:260–269.
13. Quiding-Järbrink M, Lundin BS, Lönroth H, Svennerholm AM. CD4+ and CD8+ T cell responses in Helicobacter pylori-infected individuals. Clin Exp Immunol 2001;123:81–87.
14. Zhang M, Liu M, Luther J, Kao JY. Helicobacter pylori directs tolerogenic programming of dendritic cells. Gut Microbes 2010;1:325–329.
15. Morey P, Pfannkuch L, Pang E, Boccellato F, Sigal M, Imai-Matsushima A, Dyer V, Koch M, Mollenkopf HJ, Schlaermann P, Meyer TF. Helicobacter pylori depletes cholesterol in gastric glands to prevent interferon gamma signaling and escape the inflammatory response. Gastroenterology 2018;154:1391–1404.
16. Peek RMJ, Fiske C, Wilson KT. Role of innate immunity in Helicobacter pylori-induced gastric malignancy. Physiol Rev 2010;90:831–858.
17. Wu YY, Chen JH, Kao JT, Liu KC, Lai CH, Wang YM, Hsieh CT, Tzen JT, Hsu PN. Expression of CD25(high) regulatory T cells and PD-1 in gastric infiltrating CD4(+) T lymphocytes in patients with Helicobacter pylori infection. Clin Vaccine Immunol 2011;18:1198–1201.
18. Osaki LH, Bockerstett KA, Wong CF, Ford EL, Madison BB, DiPaolo RJ, Mills JC. Interferon-γ directly induces gastric epithelial cell death and is required for progression to metaplasia. J Pathol 2019;247:513–523.
19. Sayi A, Kohler E, Hitzler I, Arnold I, Schwendener R, Rehrauer H, Müller A. The CD4+ T cell-mediated IFN-gamma response to Helicobacter infection is essential for clearance and determines gastric cancer risk. J Immunol 2009;182:7085–7101.
20. Das S, Suarez G, Beswick EJ, Sierra JC, Graham DY, Reyes VE. Expression of B7-H1 on gastric epithelial cells: its potential role in regulating T cells during Helicobacter pylori infection. J Immunol 2006; 176:3000–3009.
21. Wu YY, Lin CW, Cheng KS, Lin C, Wang YM, Lin IT, Chou YH, Hsu PN. Increased programmed death-ligand-1 expression in human gastric epithelial cells in Helicobacter pylori infection. Clin Exp Immunol 2010; 161:551–559.
22. Mitchell P, Germain C, Fiori PL, Khamri W, Foster GR, Ghosh S, Lechler RI, Bamford KB, Lombardi G. Chronic exposure to Helicobacter pylori impairs dendritic cell function and inhibits Th1 development. Infect Immun 2007;75:810–819.
23. Holokai L, Chakrabarti J, Broda T, Chang J, Hawkins JA, Sundaram N, Wroblewski LE, Peek RMJ, Wang J, Helmrath M, Wells JM, Zavros Y. Increased programmed death-ligand 1 is an early epithelial cell response to Helicobacter pylori infection. PLoS Pathog 2019;15: e1007468.
24. Reizis B. Classical dendritic cells as a unique immune cell lineage. J Exp Med 2012;209:1053–1056.
25. Satpathy AT, KC W, Albring JC, Edelson BT, Kretzer NM, Bhattacharya D, Murphy TL, Murphy KM. Zbtb46 expression distinguishes classical dendritic cells and their committed progenitors from other immune lineages. J Exp Med 2012;209:1135–1152.
26. Clemente-Casares X, Hosseinzadeh S, Barbu I, Dick SA, Macklin JA, Wang Y, Momen A, Kantores C, Aronoff L, Farno M, Lucas TM, Avery J, Zarrin-Khat D, Elsaesser HJ, Razani B, Lavine KJ, Husain M, Brooks DG, Robbins CS, Cybulsky M, Epelman S. A CD103+ conventional dendritic cell surveillance system prevents development of overt heart failure during subclinical viral myocarditis. Immunity 2017;47:974–989.
27. Salmon H, Idoyaga J, Rahman A, Leboeuf M, Remark R, Jordan S, Casanova-Acebes M, Khudoynazarova M, Agudo J, Tung N, Chakarov S, Rivera C, Hogstad B, Bosenberg M, Hashimoto D, Gnjatic S, Bhardwaj N, Palucka AK, Brown BD, Brody J, Ginhoux F, Merad M. Expansion and activation of CD103(+) dendritic cell progenitors at the tumor site enhances tumor responses to therapeutic PD-L1 and BRAF inhibition. Immunity 2016;44:924–938.
28. Choi JH, Cheong C, Dandamudi DB, Park CG, Rodriguez A, Mehandru S, Velinzon K, Jung IH, Yoo JY, Oh GT, Steinman RM. Flt3 signaling-dependent dendritic cells protect against atherosclerosis. Immunity 2011; 35:819–831.
29. Waskow C, Liu K, Darrasse-Jèze G, Guermonprez P, Ginhoux F, Merad M, Shengelia T, Yao K, Nussenzweig M. The receptor tyrosine kinase Flt3 is required for dendritic cell development in peripheral lymphoid tissues. Nat Immunol 2008;9:676–683.
30. Yun TJ, Lee JS, Machmach K, Shim D, Choi J, Wi YJ, Jang HS, Jung IH, Kim K, Yoon WK, Miah MA, Li B, Chang J, Bego MG, Pham TNQ, Loschko J, Fritz JH, Krug AB, Lee SP, Keler T, Guimond JV, Haddad E, Cohen EA, Sirois MG, El-Hamamsy I, Colonna M, Oh GH, Choi JH, Cheong C. Indoleamine 2,3-dioxygenase-expressing aortic plasmacytoid dendritic cells protect against atherosclerosis by induction of regulatory T cells. Cell Metab 2016;23:852–866.
31. Wunder C, Churin Y, Winau F, Warnecke D, Vieth M, Lindner B, Zähringer U, Mollenkopf HJ, Heinz E, Meyer TF. Cholesterol glucosylation promotes immune evasion by Helicobacter pylori. Nat Med 2006;12:1030–1038.
32. Khamri W, Moran AP, Worku ML, Karim QN, Walker MM, Annuk H, Ferris JA, Appelmelk BJ, Eggleton P, Reid KB, Thursz MR. Variations in Helicobacter pylori lipopolysaccharide to evade the innate immune component surfactant protein D. Infect Immun 2005;73:7677–7686.

33. Khamri W, Worku ML, Anderson AE, Walker MM, Hawgood S, Reid KB, Clark HW, Thursz MR. Helicobacter infection in the surfactant protein D-deficient mouse. Helicobacter 2007;12:112–123.
34. Murray E, Khamri W, Walker MM, Eggleton P, Moran AP, Ferris JA, Knapp S, Karim QN, Worku M, Strong P, Reid KBM, Thursz MR. Expression of surfactant protein D in the human gastric mucosa and during Helicobacter pylori infection. Infect Immun 2002;70:1481–1487.
35. Vange P, Bruland T, Doseth B, Fossmark R, Sousa MML, Beisvag V, Sørdal Ø, Qvigstad G, Waldum HL, Sandvik AK, Bakke I. The cytoprotective protein clusterin is overexpressed in hypergastrinemic rodent models of oxyntic preneoplasia and promotes gastric cancer cell survival. PLoS One 2017;12:e0184514.
36. Shimizu T, Choi E, Petersen CP, Noto JM, Romero-Gallo J, Piazuelo MB, Washington MK, Peek RMJ, Goldenring JR. Characterization of progressive metaplasia in the gastric corpus mucosa of Mongolian gerbils infected with Helicobacter pylori. J Pathol 2016; 239:399–410.
37. Weis VG, Sousa JF, LaFleur BJ, Nam KT, Weis JA, Finke PE, Ameen NA, Fox JG, Goldenring JR. Heterogeneity in mouse spasmolytic polypeptide-expressing metaplasia lineages identifies markers of metaplastic progression. Gut 2013;62:1270–1279.
38. Kim JJ, Nottingham LK, Sin JI, Tsai A, Morrison L, Oh J, Dang K, Hu Y, Kazahaya K, Bennett M, Dentchev T, Wilson DM, Chalian AA, Boyer JD, Agadjanyan MG, Weiner DB. CD8 positive T cells influence antigen-specific immune responses through the expression of chemokines. J Clin Invest 1998;102:1112–1124.
39. Ohtani N, Ohtani H, Nakayama T, Naganuma H, Sato E, Imai T, Nagura H, Yoshie O. Infiltration of CD8+ T cells containing RANTES/CCL5+ cytoplasmic granules in actively inflammatory lesions of human chronic gastritis. Lab Invest 2004;84:368–375.
40. Rad R, Ballhorn W, Voland P, Eisenächer K, Mages J, Rad L, Ferstl R, Lang R, Wagner H, Schmid RM, Bauer S, Prinz C, Kirschning CJ, Krug A. Extracellular and intracellular pattern recognition receptors cooperate in the recognition of Helicobacter pylori. Gastroenterology 2009;136:2247–2257.
41. Hafsi N, Voland P, Schwendy S, Rad R, Reindl W, Gerhard M, Prinz C. Human dendritic cells respond to Helicobacter pylori, promoting NK cell and Th1-effector responses in vitro. J Immunol 2004; 173:1249–1257.
42. Khamri W, Walker MM, Clark P, Atherton JC, Thursz MR, Bamford KB, Lechler RI, Lombardi G. Helicobacter pylori stimulates dendritic cells to induce interleukin-17 expression from CD4+ T lymphocytes. Infect Immun 2010;78:845–853.
43. Rizzuti D, Ang M, Sokollik C, Wu T, Abdullah M, Greenfield L, Fattouh R, Reardon C, Tang M, Diao J, Schindler C, Cattral M, Jones NL. Helicobacter pylori inhibits dendritic cell maturation via interleukin-10-mediated activation of the signal transducer and activator of transcription 3 pathway. J Innate Immun 2015; 7:199–211.
44. Hitzler I, Oertli M, Becher B, Agger EM, Müller A. Dendritic cells prevent rather than promote immunity conferred by a helicobacter vaccine using a mycobacterial adjuvant. Gastroenterology 2011;141:186–196.
45. Oertli M, Sundquist M, Hitzler I, Engler DB, Arnold IC, Reuter S, Maxeiner J, Hansson M, Taube C, Quiding-Järbrink M, Muller A. DC-derived IL-18 drives Treg differentiation, murine Helicobacter pylori-specific immune tolerance, and asthma protection. J Clin Invest 2012; 122:1082–1096.
46. Bennett CL, Clausen BE. DC ablation in mice: promises, pitfalls, and challenges. Trends Immunol 2007; 28:525–531.
47. Arnold IC, Zhang X, Urban S, Artola-Borán M, Manz MG, Ottemann KM, Müller A. NLRP3 controls the development of gastrointestinal CD11b+ dendritic cells in the steady state and during chronic bacterial infection. Cell Rep 2017;21:3860–3872.
48. Bain CC, Scott CL, Uronen-Hansson H, Gudjonsson S, Jansson O, Grip O, Guilliams M, Malissen B, Agace WW, Mowat AM. Resident and pro-inflammatory macrophages in the colon represent alternative context-dependent fates of the same Ly6Chi monocyte precursors. Mucosal Immunol 2013;6:498–510.
49. Bachem A, Güttler S, Hartung E, Ebstein F, Schaefer M, Tannert A, Salama A, Movassaghi K, Opitz C, Mages HW, Henn V, Kloetzel PM, Gurka S, Kroczek RA. Superior antigen cross-presentation and XCR1 expression define human CD11c+CD141+ cells as homologues of mouse CD8+ dendritic cells. J Exp Med 2010; 207:273–1281.
50. Guilliams M, Dutertre CA, Scott CL, McGovern N, Sichien D, Chakarov S, Van Gassen S, Chen J, Poidinger M, De Prijck S, Tavernier SJ, Low I, Irac SE, Mattar CN, Sumatoh HR, Low GHL, Chung TJK, Chan DKH, Tan KK, Hon TLK, Fossum E, Bogen B, Choolani M, Chan JKY, Larbi A, Luche H, Henri S, Saeys Y, Newell EW, Lambrecht BN, Malissen B, Ginhoux F. Unsupervised high-dimensional analysis aligns dendritic cells across tissues and species. Immunity 2016;45:669–684.
51. Gurka S, Hartung E, Becker M, Kroczek RA. Mouse conventional dendritic cells can be universally classified based on the mutually exclusive expression of XCR1 and SIRPα. Front Immunol 2015;6:35.
52. Mildner A, Jung S. Development and function of dendritic cell subsets. Immunity 2014;40:642–656.
53. Seillet C, Jackson JT, Markey KA, Brady HJ, Hill GR, Macdonald KP, Nutt SL, Belz GT. CD8α+ DCs can be induced in the absence of transcription factors Id2, Nfil3, and Batf3. Blood 2013;121:1574–1583.
54. Sugiura D. Restriction of PD-1 function by cis-PD-L1/CD80 interactions is required for optimal T cell responses. Science 2019;364:558–566.
55. Francisco LM, Salinas VH, Brown KE, Vanguri VK, Freeman GJ, Kuchroo VK, Sharpe AH. PD-L1 regulates the development, maintenance, and function of induced regulatory T cells. J Exp Med 2009;206:3015–3029.
56. Schmitt EG, Williams CB. Generation and function of induced regulatory T cells. Front Immunol 2013;4:152.

57. Silva MT. Neutrophils and macrophages work in concert as inducers and effectors of adaptive immunity against extracellular and intracellular microbial pathogens. J Leukoc Biol 2010;87:805–813.
58. Petersen CP, Mills JC, Goldenring JR. Murine models of gastric corpus preneoplasia. Cell Mol Gastroenterol Hepatol 2016;3:11–26.
59. Mera RM, Bravo LE, Camargo MC, Bravo JC, Delgado AG, Romero-Gallo J, Yepez MC, Realpe JL, Schneider BG, Morgan DR, Peek RM Jr, Correa P, Wilson KT, Blanca P. Dynamics of Helicobacter pylori infection as a determinant of progression of gastric precancerous lesions: 16-year follow-up of an eradication trial. Gut 2018;67:1239–1246.
60. Lu J, Firpi-Morell RJ, Dang LH, Lai J, Liu X. An unusual case of gastritis in one patient receiving PD-1 blocking therapy: coexisting immune-related gastritis and cytomegaloviral infection. Gastroenterology Res 2018; 11:383–387.
61. Postow MA, Sidlow R, Hellmann MD. Immune-related adverse events associated with immune checkpoint blockade. N Engl J Med 2018;378:158–168.
62. Samaan MA, Pavlidis P, Papa S, Powell N, Irving PM. Gastrointestinal toxicity of immune checkpoint inhibitors: from mechanisms to management. Nat Rev Gastroenterol Hepatol 2018;15:222–234.
63. Mackarehtschian K, Hardin JD, Moore KA, Boast S, Goff SP, Lemischka IR. Targeted disruption of the flk2/flt3 gene leads to deficiencies in primitive hematopoietic progenitors. Immunity 1995;3:147–161.
64. Latchman YE, Liang SC, Wu Y, Chernova T, Sobel RA, Klemm M, Kuchroo VK, Freeman GJ, Sharpe AH. PD-L1-deficient mice show that PD-L1 on T cells, antigen-presenting cells, and host tissues negatively regulates T cells. Proc Natl Acad Sci U S A 2004; 101:10691–10696.
65. Lee A, O'Rourke J, De Ungria MC, Robertson B, Daskalopoulos G, Dixon MF. A standardized mouse model of Helicobacter pylori Infection: introducing the Sydney strain. Gastroenterology 1997;112:1386–1397.
66. Chen XY, van der Hulst RW, Bruno MJ, van der Ende A, Xiao SD, Tytgat GN, Ten Kate FJ. Interobserver variation in the histopathological scoring of Helicobacter pylori related gastritis. J Clin Pathol 1999;52:612–615.
67. Dixon MF, Genta RM, Yardley JH, Correa P. Classification and grading of gastritis. The updated Sydney System. International Workshop on the Histopathology of Gastritis, Houston 1994. Am J Surg Pathol 1996; 20:1161–1181.
68. El-Zaatari M, Kao JY, Tessier A, Bai L, Hayes MM, Fontaine C, Eaton KA, Merchant JL. Gli1 deletion prevents Helicobacter-induced gastric metaplasia and expansion of myeloid cell subsets. PLoS One 2013;8: e58935.
69. Koh J, Kwak Y, Kim J, Kim WH. High-throughput multiplex immunohistochemical imaging of the tumor and its microenvironment. Cancer Res Treat 2020;52:98–108.

Received July 29, 2020. Accepted April 13, 2021.

Correspondence
Address correspondence to: Jae-Hoon Choi, DVM, PhD, Department of Life Sciences, College of Natural Sciences, Research Institute for Natural Sciences, Hanyang University, 222 Wangsimni-ro, Seongdong-gu, Seoul 04763, Republic of Korea. e-mail: jchoi75@hanyang.ac.kr; fax: (82) 2-2298-0319; or Dae-Yong Kim, DVM, PhD, Department of Veterinary Pathology, College of Veterinary Medicine, Seoul National University, 1 Gwanak-ro, Gwanak-gu, Seoul 08826, Republic of Korea. e-mail: daeyong@snu.ac.kr; fax: (82) 2-879-2736.

CRediT Authorship Contributions

Du-Min Go (Conceptualization: Equal; Data curation: Lead; Formal analysis: Lead; Investigation: Lead; Methodology: Lead; Validation: Lead; Visualization: Lead; Writing – original draft: Lead; Writing – review & editing: Equal)

Seung Hyun Lee (Conceptualization: Equal; Data curation: Lead; Formal analysis: Lead; Investigation: Lead; Methodology: Lead; Validation: Lead; Visualization: Lead; Writing – original draft: Lead; Writing – review & editing: Equal)

Su-Hyung Lee (Methodology: Equal)

Sang-Ho Woo (Methodology: Equal)

Kibyeong Kim (Methodology: Equal)

Kyeongdae Kim (Methodology: Equal)

Kyu Seong Park (Methodology: Equal)

Jong-Hwan Park (Resources: Equal)

Sang-Jun Ha (Resources: Equal)

Woo Ho Kim (Data curation: Equal; Formal analysis: Equal; Methodology: Equal)

Jae-Hoon Choi (Conceptualization: Lead; Data curation: Equal; Formal analysis: Equal; Funding acquisition: Lead; Investigation: Equal; Methodology: Equal; Project administration: Lead; Resources: Lead; Software: Equal; Supervision: Lead; Validation: Equal; Visualization: Equal; Writing – original draft: Lead; Writing – review & editing: Lead)

Dae-Yong Kim (Conceptualization: Lead; Data curation: Equal; Formal analysis: Equal; Funding acquisition: Lead; Investigation: Equal; Methodology: Equal; Project administration: Lead; Resources: Equal; Software: Equal; Supervision: Lead; Validation: Equal; Visualization: Equal; Writing – original draft: Equal; Writing – review & editing: Equal)

Conflicts of interest
The authors disclose no conflicts.

Funding
This research was supported by NRF-2016M3A9D5A01952416, 2016M3A9D5A01952413, 2018R1A2B6003393, and 2015M3A9B6029138, and by the National Research Foundation of the Korean government.